

A Theoretical Analysis of Detecting Large Model-Generated Time Series

Junji Hou, Junzhou Zhao*, Shuo Zhang, Pinghui Wang

MoE KLINNS Lab, Xi'an Jiaotong University, Xi'an 710049, P. R. China
{15955192, zs412082986}@stu.xjtu.edu.cn, {junzhou.zhao, phwang}@xjtu.edu.cn

Abstract

Motivated by the increasing risks of data misuse and fabrication, we investigate the problem of identifying synthetic time series generated by Time-Series Large Models (TSLMs) in this work. While there is extensive research on detecting model generated text, we find that these existing methods are not applicable to time series data due to the fundamental modality difference, as time series usually have lower information density and smoother probability distributions than text data, which limit the discriminative power of token-based detectors. To address this issue, we examine the subtle distributional differences between real and model-generated time series and propose *contraction hypothesis*, which states that model-generated time series, unlike real ones, exhibit progressively decreasing uncertainty under recursive forecasting. We formally prove this hypothesis under theoretical assumptions on model behavior and time series structure. Model-generated time series exhibit progressively concentrated distributions under recursive forecasting, leading to uncertainty contraction. We provide empirical validation of the hypothesis across diverse datasets. Building on this insight, we introduce the *Uncertainty Contraction Estimator (UCE)*, a white-box detector that aggregates uncertainty metrics over successive prefixes to identify TSLM-generated time series. Extensive experiments on 32 datasets show that UCE consistently outperforms state-of-the-art baselines, offering a reliable and generalizable solution for detecting model-generated time series.

1 Introduction

Recent advances in time series forecasting have given rise to Time Series Large Models (TSLMs), which are pre-trained on massive multi-domain time series datasets with billions of parameters (Ansari et al. 2024; Liu et al. 2024; Shi et al. 2025). The vast training data and enormous parameter scale enable TSLMs to achieve remarkable long-term zero-shot forecasting on entirely new datasets or domains without any labeled examples or task-specific fine-tuning, as evidenced by recent scaling law analyses (Yao et al. 2025). Leveraging these sophisticated forecasting capabilities, TSLMs have demonstrated strong performance in domains such as finance, Internet of Things (IoT), and climate science.

The powerful capability of TSLMs raises significant concerns about potential data fabrication or misuse. Unlike classical approaches (e.g., ARIMA, LSTM), which degrade in performance outside their training domains, TSLMs can generate coherent long sequences even for unfamiliar domains. If maliciously exploited, this capability could enable the systematic fabrication of time series and pose severe threats in scenarios where data authenticity is critical.

- **Finance:** TSLMs can synthesize long transaction histories that mirror real trading patterns, facilitating fraudulent activities such as inflated valuations or hidden manipulations, such as those seen in the 2012 LIBOR scandal (Gupta 2024; Rose and Sesia 2013).
- **Scientific Research:** Highly realistic counterfeit measurement time series (e.g., signal traces or biological data) can distort experimental outcomes, similar to Schön and Wakefield data forgeries (Brumfiel 2002; Godlee, Smith, and Marcovitch 2011).
- **Environmental Governance:** Attackers can generate counterfeit metrics (e.g., air quality indices or emissions) that reproduce genuine diurnal and seasonal cycles to conceal pollution spikes or overstate improvements, misleading policy makers and obscuring real hazards (Wang, Wang, and Wilkes 2021).

To address these threats, we introduce a theoretical framework for white-box detection of TSLM-generated time series. Since there are no dedicated detection methods for time series data, we adapt text-based detection methods to time series data. Textual detectors exploit the observation that LLMs exhibit different token-level probability patterns on human-written and model-generated text, and therefore typically build zero-shot classifiers from each token’s probability or its rank within the model’s vocabulary. However, these methods face significant challenges when applied to time series because of fundamental modality differences.

Textual data exhibit structural semantics and carry rich token-level information (Meister et al. 2022), which creates greater semantic distances among different tokens. In any given context, only a small subset of tokens is semantically plausible and with higher probability (e.g., probabilities might concentrate on “apple”, “orange” given the prefix “I eat an”). This produces sharper, low-entropy probability distributions over the vocabulary, with a narrower range of

*Corresponding Author.

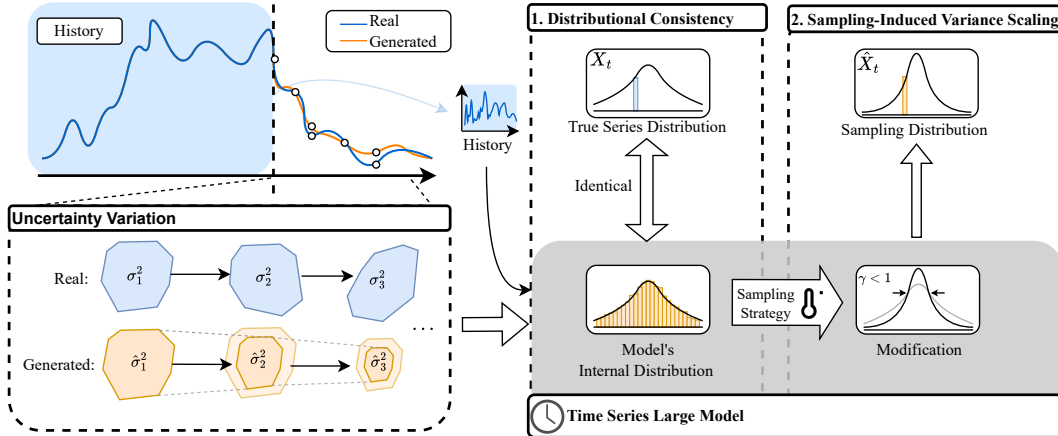


Figure 1: Illustration of the variation in uncertainty for real and model-generated time series.

token selection.

In contrast, time series carry less information at each point (Nie et al. 2023) and inherently contain greater intrinsic uncertainty, yielding smoother probability distributions. Notably, despite the greater entropy of these smooth distributions, they reflect the information at each time point rather than specific values. Since the adjacent values in time series are highly similar (e.g. temperature 25.1°C and 25.2°C), resulting in large mutual information, time series values convey less information. Consequently, text-based detectors that rely on token probabilities perform poorly on time series given the relatively lower probability gaps between values.

Since point-wise probabilities are insufficiently discriminative in time series, we instead analyze the full distributions from the model. We show that a TSLM’s internal distributions, conditioned on the full history, accurately capture the true series distributions and their inherent uncertainty. As TSLMs are trained to minimize prediction errors, the internal distributions are concentrated via model’s sampling strategies for forecasting. In recursive forecasting, the uncertainty is cumulatively decreasing, leading to progressively concentrated internal distributions, as illustrated in Fig. 1.

We therefore propose the **contraction hypothesis**, namely, TSLM-generated time series exhibit progressively decreasing uncertainty, whereas real time series do not. To validate this hypothesis, we provide a theoretical analysis under idealized assumptions on model behavior and time series structure (see Section 4.2) with empirical evidence through long-horizon forecasting experiments (see Fig. 2). Grounded in this detailed analysis of properties unique to time series, we introduce the Uncertainty Contraction Estimator (UCE), a white-box model generation detection method for time series data. UCE captures uncertainty dynamics from internal prediction distributions and identifies sequences with lower uncertainty levels as model-generated.

Our main contributions are summarized as follows.

- To the best of our knowledge, we present the first framework for white-box detection of TSLM-generated time series. We analyze the detailed properties unique to time

series in contrast to textual data and address the challenge of low information density in time series.

- We propose the contraction hypothesis, which states that model-generated time series exhibit progressively decreasing uncertainty during recursive forecasting, whereas real series do not. We provide a theoretical analysis under idealized assumptions of time series and model and empirically validate it.
- Based on this hypothesis, we develop the Uncertainty Contraction Estimator (UCE), which captures uncertainty dynamics over successive prefixes using TSLMs to distinguish model-generated from real time series.

2 Related Work

2.1 Time Series Large Models

Time series large models have emerged to significantly advance zero-shot time series forecasting. Earlier methods such as PromptCast (Xue and Salim 2023) and LLM-Time (Nate et al. 2023) directly leverage LLMs for time series. They convert time series data into text-based prompts and use pretrained LLMs with little to no task-specific adaptation. Such methods require dataset-specific templates and rely heavily on model scale.

PatchTST (Nie et al. 2023) introduces splitting time series into patch embeddings, a technique later adopted in models such as GPT4TS (Zhou et al. 2023) and Time-LLM (Jin et al. 2024). These methods use patch embeddings as inputs to LLMs for prediction, but require extensive fine-tuning. Moreover, their performance and inference efficiency have been questioned (Tan et al. 2024).

Recent work concentrates on models trained on vast and diverse time series datasets. MOMENT (Goswami et al. 2024) employs uniform random masking to generate patch embedding for self-supervised pretraining. Chronos (Ansari et al. 2024) discretizes real-valued time series through scaling and quantization for forecasting and introduces data augmentation to improve generalization. Timer (Liu et al. 2024) adopts a decoder-only transformer architecture, enabling multiple temporal tasks such as forecasting, anomaly

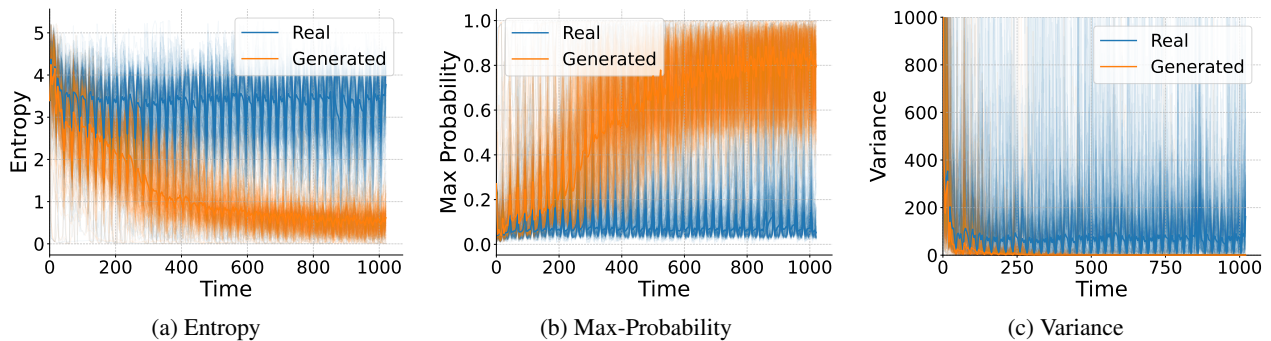


Figure 2: The empirical results show the trajectories of uncertainty metrics, including entropy (2a), max-probability (2b) and variance (2c) of both real and model-generated time series data, illustrating reduction in uncertainty for generated data.

detection, and imputation. Time-MoE (Shi et al. 2025) leverages a Mixture-of-Experts framework to improve forecasting performance and enhance cross-domain generalization while maintaining computational efficiency. These methods collectively represent the emerging trend of general-purpose time series models capable of handling diverse tasks with minimal or no fine-tuning.

2.2 Model Generation Detection

The growing generative capabilities of LLMs have raised concerns about distinguishing model-generated content, particularly in the textual domain. Early work on model generation detection conduct supervised classification using bag of words (Solaiman et al. 2019) or neural representations (Jawahar, Abdul-Mageed, and Lakshmanan 2020; Uchendu et al. 2020), but often overfit and underperform on out-of-distribution data (Pu et al. 2023). To overcome this limitation, zero-shot detectors use LLM output statistics, such as perplexity (Lavergne, Urvoy, and Yvon 2008) and log rank (Gehrmann, Strobel, and Rush 2019; Hashimoto, Zhang, and Liang 2019).

Recent work analyzes token probabilities and uses the discrepancies between human-written and model-generated text to develop classifiers. DetectGPT (Mitchell et al. 2023), Fast-DetectGPT (Bao et al. 2023), and NPR (Su et al. 2023) compare probability differences between perturbed texts, while DNA-GPT (Yang et al. 2024) leverages regeneration to compute divergence. FourierGPT (Xu et al. 2024) performs a spectral analysis on token probability sequences to extract linguistic features that distinguish human-authored from model-generated text. Binocular (Hans et al. 2024) leverages both an observer and a performer to compute cross-perplexity and isolate intrinsic prefix-induced uncertainty to improve detection accuracy. Black-box methods such as intrinsic dimension (Tulchinskii et al. 2023) perform topological data analysis over token embeddings and find that human-written texts are more complicated in topology.

Despite their success in text, these methods rely on the dense and discrete structure of the language, making them unsuitable for continuous and information-sparse time series data. In this work, we extend zero-shot model generation detection to time series by introducing uncertainty-based met-

rics derived from model’s internal probability distributions.

3 Problem Formulation and Preliminaries

In this section, we formally define the model-generated time series detection problem. Then we provide some preliminaries about our framework.

3.1 Problem Formulation

Let $\mathbf{X}_t = (X_1, \dots, X_t)$ denote a univariate time series with *unknown* history. We perform a zero-shot classification of \mathbf{X}_t as real or model-generated without labeled examples.

We assume a white-box setting with access to the model’s internal probability distribution $p_\theta(\cdot|\mathbf{X}_t)$ rather than to the model architecture or parameters θ . Our detection employs point-wise probabilistic TSLMs over an equidistant vocabulary $\mathcal{V} = \{v_i | v_{i+1} - v_i = \Delta, -R \leq v_i \leq R\}$ for new token sampling. Therefore, sampling token v_i yields the numerical forecast $\hat{X}_t = v_i$. In the limit $\Delta \rightarrow 0$ and $R \rightarrow \infty$, \mathcal{V} converges to the real set \mathbb{R} and a probability density function f_θ is obtained. Such a formulation allows for detection evaluation across diverse model architectures.

Some frequently used symbols throughout the paper are given in Table 1. In the following sections, we use probability density functions to refer to the distributions.

3.2 Preliminaries

We first introduce some assumptions and premises about time series and idealized TSLMs. Detailed definitions and assumptions are provided in the Appendix.

We formally model time series as realizations of stochastic processes, where each observation sequence is a sample path of this process. We decompose the real time series process at time point t into two components (Box et al. 1978):

$$X_t = T_t + n_t, \quad n_t \sim \mathcal{N}(0, \sigma_t^2),$$

where T_t denotes the trend sequence, representing predictable components, and n_t is a Gaussian process with zero mean and variance such that $\sigma_t^2 = \sum_{i=1}^t \alpha_i \sigma_{t-i}^2$, $\sum_{i=1}^t \alpha_i = 1$. The noise process represents the unpredictable or uncertainty components.

Symbol	Description
X_t, \hat{X}_t	Real / forecast time series process
T_t	Deterministic trend component at time t
n_t, \hat{n}_t	True / forecast (Gaussian) noise at time t
$\mathbf{X}_{-H:t}, \hat{\mathbf{X}}_{-H:t}$	History X_{-H}, \dots, X_t (or $\hat{X}_{-H}, \dots, \hat{X}_t$)
$f_t(X_t), \hat{f}_\theta(\hat{X}_t)$	Probability density of X_t / \hat{X}_t at time t
$\sigma_t^2, \hat{\sigma}_t^2$	Variance of true noise n_t / forecast noise \hat{n}_t
$f_\theta(z_t \mathbf{X}_{-H:t-1})$	Model's internal probability density with history $\mathbf{X}_{-H:t-1}$, abbreviated as $f_\theta(z_t)$
$\tilde{\sigma}_t^2$	Variance of internal probability distribution at time t
γ_t	Scaling factor of sampling strategy to $f_\theta(z_t)$ at time t

Table 1: Some frequently used symbols

We introduce *Ideal Model*, which, for any real-valued time series in \mathbb{R} , predicts probability distributions to minimize the expectation of cross-entropy loss. Conceptually, it generalizes practical TSLMs by letting both training data and model capacity grow without bound. This abstraction allows us to derive fundamental detection principles regardless of specific architectures or training constraints.

We formalize *model evaluation function* as Eq. (1):

$$\text{Eva} = \left[\sum_{i=1}^{\tau} g \left(\left| X_i - \hat{X}_i \right|^p \right) \right]^{\frac{1}{p}}, 1 \leq p \leq \infty, \quad (1)$$

where g is any non-negative strictly increasing mapping. Specifically, if g is linear, Eva reduces to the standard ℓ_p norm of point-wise errors (e.g., RMSE when $p = 2$). Since X_i and \hat{X}_i are variables, Eva is also a variable. Eva is a unified form of various model prediction evaluators (e.g., MSE, MAE) which in turn guides the model generation process.

4 Methodology

In this section, we introduce the Uncertainty Contraction Estimator (UCE), a novel time series model generation detection method. We first establish the theoretical foundation by proposing the *contraction hypothesis* in Section 4.1, followed by a formal analysis in Section 4.2. Finally, the implementation details of UCE are presented in Section 4.3.

4.1 Contraction Hypothesis

UCE hinges on two observations: (1) the model's internal distributions faithfully reproduce true series distributions at each time; (2) through sampling strategies, the model systematically modifies these distributions, creating a self-reinforcing process of exponentially decreasing uncertainty. We formalize these insights as the contraction hypothesis.

Contraction hypothesis: TSLM-generated time series exhibit progressively concentrating internal distributions with decreasing uncertainty, whereas real series do not.

The term ‘‘contraction’’ refers to the contraction mapping nature of the uncertainty reduction. We systematically

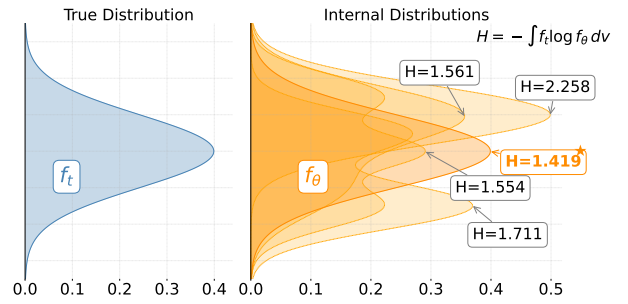


Figure 3: Comparison of the true distribution (blue) and model's internal distributions (orange). For an ideal model, its internal distribution coincides with the true distribution.

substantiate the hypothesis through a tripartite theoretical framework. Formal proofs of all the following propositions are provided in the Appendix.

4.2 Theoretical Analysis

Distributional Consistency. We begin with the property of ideal models. Given any history $\mathbf{X}_{-H:t-1}$, TSLM generates an *internal probability distribution* f_θ . From the perspective of this distribution, we revisit the ideal models and conclude the distribution-perfect prediction property.

Lemma 4.1. For $\sigma_t^2 \geq 0$, we have $f_\theta \equiv f_t$ a.e.

Fig. 3 illustrates the insight of Lemma 4.1. Since the probability density of $X_t = T_t + d$ is $f_t(T_t + d)$, the loss expectation is therefore the cross entropy $-\int f_t(v) \log f_\theta(v) dv$ between f_θ and the true series distribution f_t . As illustrated in Fig. 3, it is minimized when $f_\theta \equiv f_t$ almost everywhere by Gibbs' inequality. Specifically, if the true sequence is entirely deterministic (i.e., zero uncertainty), ideal models make value-perfect predictions, leading to Corollary 4.2.

Corollary 4.2. If $\sigma_t^2 = 0$, we have $f_\theta(z = v) = \delta(v - T_t)$, where δ is the Dirac- δ function.

In summary, the ideal model's internal distributions coincide with true series distributions and therefore preserve the inherent uncertainty in the series.

Sampling-Induced Variance Scaling. Using the property of ideal models to reproduce true series distributions, we analyze the prediction of $\hat{\mathbf{X}}_{1:\tau}$ with history $\mathbf{X}_{-H:0}$, and focus on the variation in uncertainty. In this section, we explain that the sampling probability distribution \hat{f}_t of each X_t is a modified version of f_θ , which tends to reduce its uncertainty.

TSLMs modify internal distributions f_θ through sampling strategies to modulate output diversity (Radford et al. 2019). We summarize common sampling strategies as follows: (1) scaling (e.g., temperature sampling); and (2) symmetric truncation (with normalization, e.g., top- k). These modifications preserve the means of f_θ but alter their variances, as shown in Fig. 4, generating sampling probability distributions $\hat{f}_\theta(\hat{X}_t = v)$ to sample X_t with variance $\hat{\sigma}_t^2$.

Let the uncertainty (variance) of f_θ be σ_t^2 at time t , we denote the modified uncertainty by sampling strategies as

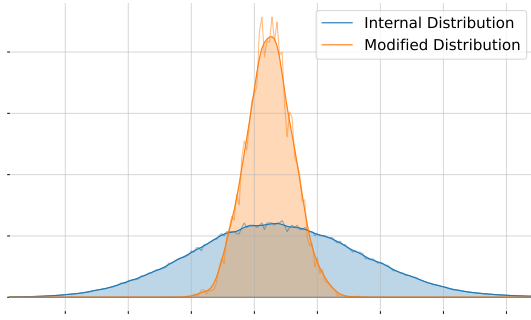


Figure 4: Comparison of the internal distribution (blue, from the model logits) and modified sampling distribution (orange, from 10,000-step Monte Carlo) for a single prediction step. The model’s internal probability distribution becomes sharper under our sampling strategy.

$\hat{\sigma}_t^2 = \gamma_t \cdot \tilde{\sigma}_t^2$. Intuitively, γ_t controls uncertainty expansion ($\gamma_t > 1$), preservation ($\gamma_t = 1$), or contraction ($\gamma_t < 1$). Since modifications of sampling strategies preserve the expectation, we recursively obtain $\mathbb{E}(\hat{X}_t) = T_t$ for all $1 \leq t \leq \tau$. We therefore treat the generation of $\hat{\mathbf{X}}_{1:\tau}$ as τ independent, one-step predictions given their respective histories. We evaluate the differences between $\mathbf{X}_{1:\tau}$ and $\hat{\mathbf{X}}_{1:\tau}$ using the model evaluation function, leading to Lemma 4.3.

Lemma 4.3. *The expectation of the model evaluation function $\mathbb{E}(\text{Eva})$ increases monotonically with respect to all $\hat{\sigma}_t$.*

Lemma 4.3 indicates that a smaller $\hat{\sigma}_t^2$ yields a lower Eva value, suggesting a higher quality of generation. Given $\hat{\sigma}_t^2 = \gamma_t \cdot \tilde{\sigma}_t^2$, when $\tilde{\sigma}_t^2$ is fixed, a smaller γ_t yields lower $\mathbb{E}(\text{Eva})$, which validates our intuition.

In particular, we derive a corollary from Lemma 4.3 that if metrics such as MSE are used as training loss, the contraction of uncertainty is immediate.

Corollary 4.4. *If the loss function is defined in the same form as the model evaluation function Eva in Eq. (1) (e.g., MSE), we have $f_\theta(z = v) = \delta(v - T_t)$.*

Based on the analysis, we intuitively expect that TSLMs employ $\gamma_t < 1$ in practice. In the following, we further analyze this intuition of γ_t in terms of performance.

Recursive Variance Reduction. With the intuition of γ_t above, we examine how the sampling distribution (i.e., the internal distribution modified by γ_t) affects the subsequent generation. In this section, we demonstrate the recursive evolution of the variance and analyze its behavior under different values of the scaling factor γ_t .

According to Lemma 4.1, the ideal model reproduces any distribution with variance satisfying $\sigma_t^2 = \sum_{i=1}^l \alpha_i \sigma_{t-i}^2$. When forecasts $\hat{X}_1, \hat{X}_2, \dots$ serve as histories, their variances $\hat{\sigma}_1^2, \hat{\sigma}_2^2, \dots$ also follow the same recurrence relation.

$$\tilde{\sigma}_t^2 = \sum_{i=1}^l \alpha_i \hat{\sigma}_{t-i}^2 = \sum_{i=1}^l \alpha_i \gamma_{t-i} \tilde{\sigma}_{t-i}^2, \quad \sum_{i=1}^l \alpha_i = 1. \quad (2)$$

Typically, the uncertainty scaling behavior is consistent and $\gamma_t < 1$ or $\gamma_t > 1$ for all t . When $\gamma_t < 1$, the internal uncertainty, according to Eq. (2), is strictly lower than the weight sum of historical uncertainties, leading to an exponential decay in uncertainty towards 0. By Corollary 4.2, the forecast series \hat{X}_t converges to the trend T_t . Conversely, when $\gamma_t > 1$, the uncertainty grows exponentially towards infinity, introducing excessive noise into the forecast that undermines trend capture and violates forecasting objectives. When $\gamma_t \equiv 1$, the uncertainty in forecast series is relatively stable for ideal models, which is unattainable for practical models due to noise accumulation.

This theoretical analysis also helps explain why many practical TSLMs exhibit similar behaviors of uncertainty contraction. For example, Chronos (Ansari et al. 2024) adopts contractive sampling strategies by using top- k with median sampling, and therefore $\gamma_t < 1$ holds consistently. Timer (Liu et al. 2024) and Time-MoE (Shi et al. 2025) utilize point-wise errors (e.g., MSE) as training loss, sharing the form as Eva defined in Eq. (1). According to Corollary 4.4, the forecast uncertainty converges rapidly, indicating their equivalence to $\gamma_t < 1$ in terms of performance. We formalize the aforementioned analysis as *contraction hypothesis*, where variance can be substituted for other metrics.

Theorem 4.5. *For an Ideal Model’s forecast time series $\hat{\mathbf{X}}_t$ with history $\mathbf{X}_{-H:0}$, let the internal probability distribution at t be $f_\theta(z_t)$, and define its uncertainty measure by variance $\tilde{\sigma}_t^2$. Therefore we have that $\tilde{\sigma}_t^2$ is monotonically decreasing with t and $\lim_{t \rightarrow \infty} \tilde{\sigma}_t^2 \approx 0$.*

We provide empirical verification of Theorem 4.5 in Figure 2, which illustrates this uncertainty contrast over 1024 tokens using three metrics, namely entropy, max-probability, and variance, which are used in our detection method. In model-generated series, max-probability steadily approaches 1, while both entropy and variance decay towards 0. In contrast, real sequences remain comparatively stable in uncertainty. This observed discrepancy in series uncertainty, combined with the ability of TSLMs to capture it, forms the basis of our detection methodology.

4.3 Uncertainty Contraction Estimator

The Uncertainty Contraction Estimator (UCE) operationalizes the Contraction Hypothesis by quantifying the uncertainty contraction in model-generated time series. Given a candidate \mathbf{X}_t , we first sample N time points t_1, t_2, \dots, t_N with a fixed interval $\Delta t = t_{i+1} - t_i$. For each t_i , UCE takes \mathbf{X}_{t_i} as the input to the TSLM and computes its internal probability distribution \hat{P}_{t_i} as defined in Eq. (3), yielding a sequence of internal distributions.

$$\hat{P}_{t_i} = p_\theta(\cdot | X_1, \dots, X_{t_i}), \quad i = 1, \dots, N. \quad (3)$$

By Lemma 4.1 the internal probability distribution coincides with the underlying Gaussian noise distribution, which is unimodal and relatively probability-concentrated. Therefore, UCE focuses on a neighborhood \mathcal{U} around the mean. Within \mathcal{U} , UCE computes three uncertainty measures to capture different aspects of the distribution concentration.

log p(x)	0.747	0.152	0.656	0.170
Rank	0.757	0.134	0.693	0.209
LogRank	0.790	0.187	0.669	0.216
DetectGPT	0.543	0.019	0.645	0.096
Fast-DetectGPT	0.712	0.096	0.660	0.180
DetectLLM-LLR	0.815	0.324	0.705	0.233
DetectLLM-NPR	0.727	0.129	0.672	0.174
DNA-GPT	0.595	0.107	0.493	0.073
IntrinsicDim	0.631	0.084	0.653	0.154
FourierGPT	0.528	0.030	0.505	0.123
Binocular	0.523	0.035	0.597	0.037
UCE-Entropy	0.855	0.447	0.731	0.286
UCE-MaxProb	0.840	0.441	0.729	0.306
UCE-Variance	0.849	0.325	0.634	0.227
	In-Dist AUROC	In-Dist TPR	Zero-Shot AUROC	Zero-Shot TPR

Figure 5: Average AUROC and TPR (at 1% FPR) for model generation detection on In-Distribution (12 datasets) and Zero-Shot (20 datasets) scenarios.

1. *Entropy* $E = -\sum_{x \in \mathcal{U}} \hat{P}(x) \log \hat{P}(x)$, which captures the spread of probability mass.
2. *Max-Probability* $P_{\max} = \max_{x \in \mathcal{U}} \hat{P}(x)$, where larger values imply lower uncertainty.
3. *Variance* $\text{Var} = \sum_{x \in \mathcal{U}} (x - \mu)^2 \hat{P}(x)$ with μ the local mean to quantify concentration.

For a selected metric $s \in \{E, P_{\max}, \text{Var}\}$, UCE calculates the metric sequence $s_{t_1}, s_{t_2}, \dots, s_{t_N}$, and the overall UCE score is their mean, formulated as $\text{UCE} = \frac{1}{N} \sum_{i=1}^N s_{t_i}$.

5 Experiments

5.1 Experimental Settings

Model and Datasets. We evaluate all detection methods using Chronos-T5 (large), a point forecasting TSLM that discretizes continuous values over a fixed token vocabulary and produces probability distributions. We conduct experiments on 32 datasets across diverse domains (energy, finance, transportation), categorized as (1) in-distribution datasets, including 12 used during Chronos training; and (2) zero-shot datasets, consisting of 20 previously unseen datasets. The zero-shot setting evaluates the generalization of detection to unseen datasets to eliminate the effects of data leakage, and validates the “black-box” detection capability (see Section 5.3). For each dataset, we follow the default setup in Chronos to generate forecasts of horizon $H = 64$, and use the corresponding H observations as ground truth. We treat forecast series as positive (model-generated) samples and real series as negative samples.

Baselines. We compare UCE with 10 text-based baselines adapted for time series: (1) **DNA-GPT WScore** (Yang et al. 2024), which measures the average log-likelihood gap between regenerated and original text given a fixed

prefix; (2) **DetectGPT** (Mitchell et al. 2023) and its efficient variant **Fast-DetectGPT** (Bao et al. 2023), which detect generation by measuring probability changes under model-guided perturbations; (3) **DetectLLM** (Su et al. 2023), using Log-Likelihood Log-Rank Ratio (LRR) and Normalized Perturbed log-Rank (NPR) metrics; (4) **Intrinsic Dimension** (Tulchinskii et al. 2023), which classifies sequences by estimating the topological “intrinsic dimension” of token embeddings; (5) **FourierGPT** (Xu et al. 2024), performing spectral analysis on token probability sequence; (6) **Binocular** (Hans et al. 2024), leveraging two models to reduce the intrinsic perplexity of prefixes; and (7) **Traditional metrics** (Gehrmann, Strobelt, and Rush 2019; Jawahar, Abdul-Mageed, and Lakshmanan 2020; Solaiman et al. 2019), including log-likelihood $\log p(x)$, rank, and log-rank. The details of the baselines are documented in the Appendix.

Evaluation Metrics. We use the Area Under the ROC Curve (AUROC) to evaluate the detection performance of UCE and the baseline methods. Since AUROC masks performance at low false positive rates (FPR), which are critical in generation detection tasks (Carlini et al. 2022; Krishna et al. 2023; Yang et al. 2024), we also report the true positive rate (TPR) at a fixed FPR of 1% (Roberts et al. 2024).

5.2 Overall Result

We evaluate detection performance under in-distribution and zero-shot settings. UCE consistently achieves state-of-the-art AUROC and TPR across all scenarios, with key results shown in Fig. 5.

In-Distribution. UCE-Entropy achieves an AUROC of 0.855, outperforming the strongest baseline, DetectLLM-LLR (0.815), by 0.040, and exceeding the baseline average (0.670) by 0.183. Its TPR reaches 0.447, surpassing DetectLLM-LLR (0.324) by 0.123 and the baseline average (0.118) by 0.329.

Zero-Shot. In the zero-shot setting, UCE-Entropy achieves an AUROC of 0.731, outperforming DetectLLM-LLR (0.705) by 0.026 and the baseline average (0.632) by 0.099. It also attains a TPR of 0.286, exceeding DetectLLM-LLR (0.233) by 0.053 and the average baseline (0.151) by 0.135.

The other two UCE metrics (Max-Probability and Variance) also show strong performance, with UCE-MaxProb approaching UCE-Entropy in TPR despite a modest AUROC gap; UCE-Variance is slightly weaker in TPR. Overall, UCE-Entropy remains the top performer, UCE-MaxProb is a close second, and UCE-Variance may offer greater robustness under alternative conditions. The full experimental results, with additional experiments, are provided in the Appendix. The experimental results suggest potential future work on hybrid or adaptive variant selection.

5.3 Cross-Model Detection Performance of UCE

In this section, we evaluate the generalization of UCE on time series generated by two alternative TSLMs, Timer and Time-MoE. We conduct experiments on 9 datasets covering multiple lengths and report both AUROC and TPR.

Time Series Length H	UCE-Entropy		UCE-Max Prob		UCE-Variance	
	AUROC	TPR	AUROC	TPR	AUROC	TPR
$H = 96$	0.833	0.301	0.556	0.041	0.635	0.108
$H = 192$	0.771	0.280	0.508	0.050	0.576	0.102
$H = 336$	0.765	0.305	0.484	0.032	0.564	0.093
$H = 768$	0.788	0.366	0.542	0.096	0.602	0.179

Table 2: AUROC and TPR (at 1% FPR) for Timer generation detection on 9 datasets.

Time Series Length H	UCE-Entropy		UCE-Max Prob		UCE-Variance	
	AUROC	TPR	AUROC	TPR	AUROC	TPR
$H = 96$	0.829	0.320	0.717	0.292	0.745	0.316
$H = 192$	0.890	0.392	0.773	0.420	0.806	0.422
$H = 336$	0.957	0.611	0.810	0.475	0.856	0.511
$H = 720$	0.950	0.561	0.845	0.540	0.863	0.566

Table 3: AUROC and TPR (at 1% FPR) for Time-MoE generation detection on 9 datasets.

UCE achieves strong overall performance on both models, with the Entropy variant exhibiting particularly notable results, consistently achieving high AUROC and TPR across both models, as shown in Table 2 and Table 3. The Max-Probability and Variance variants yield weaker performance, especially for Timer-generated sequences. Notably, UCE performs particularly well in Time-MoE, possibly due to its Mixture-of-Experts architecture with better long-forecasting performance. In Section 4.2 we show that although Timer and Time-MoE are not probabilistic forecasting models, they also exhibit uncertainty contraction, and uncertainty metrics demonstrate discriminative power between real and model-generated series.

Furthermore, the performance of UCE on both zero-shot datasets and cross-model settings also implies its potential for the “black-box” detection analogous to DetectGPT. Specifically, given a time series that originates from an unknown model and unknown source (or the real world), UCE can perform detection by leveraging a locally deployed probabilistic model to compute uncertainty-based signals.

6 Discussion

Our methodology is based on the contraction hypothesis, which depends on certain idealized assumptions (see Section 4.1). Despite the empirical support for the hypothesis from the experimental results, we revisit the foundational assumptions to strengthen our theoretical analysis.

6.1 Idealized Model Assumption

To establish an architecture-agnostic detection methodology, we postulate a theoretically optimal Ideal Model. This abstraction avoids model-specific details to identify general behaviors, but is mathematically unrealizable in practice. Existing TSLMs are approximations of this ideal, which undermine both the guarantee of perfect prediction (see Corollary 4.2) and the model’s ability to faithfully recover the true

series distribution (see Lemma 4.1). Despite the limitation, practical models also exhibit similar uncertainty contraction behaviors in forecasting.

In particular, TSLMs are trained on finite datasets with finite parameters. Since the noise samples are limited and the model is trained to minimize expected loss over these few realizations, it cannot fully capture the underlying noise distribution or the true trend. Therefore, both the estimated trend \hat{T}_t and noise \hat{n}_t inevitably deviate from the truth, and the trend deviation $\Delta T_t = |T_t - \hat{T}_t|$ accumulates as forecasting progresses. Given this non-zero deviation, Lemma 4.3 does not strictly hold, and reducing forecast variance $\hat{\sigma}_t^2$ does not always improve evaluation performance. Nevertheless, a moderate reduction in uncertainty constrains the expected evaluation error within the relatively small bound ΔT_t by concentrating probability between T_t and \hat{T}_t . As the deviation grows, greater uncertainty does not yield sufficiently better performance by correcting the error and may result in unstable forecasts. This indicates that practical TSLMs also inherently exhibit a forecasting uncertainty contraction (i.e., $\gamma_t < 1$), especially under recursive noise accumulation, as elaborated in Section 4.2. Hence, the contraction hypothesis still holds for practical models, allowing UCE to track predictive uncertainty across recursive steps.

6.2 Gaussian Noise Assumption

In this work, we assume Gaussian noise for analytical simplification: the sum of independent Gaussian noises remains Gaussian, and the variance fully characterizes the distribution. Crucially, our proofs do not depend on the exact form of the Gaussian but only require the noise to be unimodal (greatest probability for trend), symmetric (equivalence for both positive and negative biases), and having a finite second moment (existence of variance). By the additivity of the variance for independent variables, our results naturally extend to such noise models. These properties are shared by most noise models commonly assumed in real-world time series analysis (e.g., Laplacian), and the experimental results (see Appendix) validate the broad applicability of the contraction hypothesis under various noise types.

6.3 Modality Difference Analysis

In this work, we extend textual detection methods to time series via UCE. Although uncertainty metrics (e.g., entropy) are relatively simple, we investigate the unique properties of time series versus text modalities (see Section 4.2) to prove the optimality of uncertainty in discriminative power.

7 Conclusion

We investigate detecting TSLM-generated time series and hypothesize that they exhibit progressively decreasing uncertainty—unlike real data. Building on this, we propose the Uncertainty Contraction Estimator (UCE), which captures uncertainty to distinguish model-generated from real series and is validated both theoretically and empirically. Future work will further analyze the hypothesis under diverse model architectures and extend UCE to multivariate and batch-forecasting settings.

Acknowledgements

This work was supported in part by National Key Research and Development Plan in China (2023YFC3306100) and National Natural Science Foundation of China (62272372).

References

- Ansari, A. F.; Stella, L.; Turkmen, C.; Zhang, X.; Mercado, P.; Shen, H.; Shchur, O.; Rangapuram, S. S.; Pineda Arango, S.; Kapoor, S.; Zschiegner, J.; Maddix, D. C.; Mahoney, M. W.; Torkkola, K.; Gordon Wilson, A.; Bohlke-Schneider, M.; and Wang, Y. 2024. Chronos: Learning the Language of Time Series. *Transactions on Machine Learning Research*.
- Bao, G.; Zhao, Y.; Teng, Z.; Yang, L.; and Zhang, Y. 2023. Fast-DetectGPT: Efficient Zero-Shot Detection of Machine-Generated Text via Conditional Probability Curvature. In *Proceedings of the International Conference on Learning Representations*.
- Bollerslev, T. 1986. Generalized autoregressive conditional heteroskedasticity. *Journal of Econometrics*, 31(3): 307–327.
- Box, G. E. P.; Jenkins, G. M.; Reinsel, G. C.; and Ljung, G. M. 1978. *Time Series Analysis: Forecasting and Control*. Wiley.
- Brumfiel, G. 2002. Bell labs launches inquiry into allegations of data duplication. *Nature*, 417(6892): 367–368.
- Carlini, N.; Chien, S.; Nasr, M.; Song, S.; Terzis, A.; and Tramèr, F. 2022. Membership Inference Attacks From First Principles. In *IEEE Symposium on Security and Privacy*, 1897–1914.
- Chung, S.; and Siegelmann, H. T. 2021. Turing Completeness of Bounded-Precision Recurrent Neural Networks. In *Advances in Neural Information Processing Systems*, 28431–28441.
- Gehrmann, S.; Strobelt, H.; and Rush, A. M. 2019. GLTR: Statistical Detection and Visualization of Generated Text. In *Proceedings of the 57th Annual Meeting of the Association for Computational Linguistics: System Demonstrations*, 111–116.
- Godlee, F.; Smith, J.; and Marcovitch, H. 2011. Wakefield’s article linking MMR vaccine and autism was fraudulent. *BMJ (Clinical research ed.)*, 342: c7452.
- Goswami, M.; Szafer, K.; Choudhry, A.; Cai, Y.; Li, S.; and Dubrawski, A. 2024. MOMENT: A Family of Open Time-series Foundation Models. In *Proceedings of the International Conference on Learning Representations*.
- Gupta, M. 2024. Defending Against LLM-Based Financial Fraud: Best Practices and Recommendations. Accessed: 2025-07-08.
- Hans, A.; Schwarzschild, A.; Cherepanova, V.; Kazemi, H.; Saha, A.; Goldblum, M.; Geiping, J.; and Goldstein, T. 2024. Spotting LLMs with binoculars: zero-shot detection of machine-generated text. In *Proceedings of the International Conference on Machine Learning*.
- Hashimoto, T. B.; Zhang, H.; and Liang, P. 2019. Unifying Human and Statistical Evaluation for Natural Language Generation. In *Proceedings of the 2019 Conference of the North American Chapter of the Association for Computational Linguistics: Human Language Technologies*, 1689–1701.
- Jawahar, G.; Abdul-Mageed, M.; and Lakshmanan, L. 2020. Automatic Detection of Machine Generated Text: A Critical Survey. In *Proceedings of the 28th International Conference on Computational Linguistics*, 2296–2309.
- Jin, M.; Wang, S.; Ma, L.; Chu, Z.; Zhang, J. Y.; Shi, X.; Chen, P.; Liang, Y.; Li, Y.; Pan, S.; and Wen, Q. 2024. Time-LLM: Time series forecasting by reprogramming large language models. In *Proceedings of the International Conference on Learning Representations*.
- Krishna, K.; Song, Y.; Karpinska, M.; Wieting, J.; and Iyyer, M. 2023. Paraphrasing evades detectors of AI-generated text, but retrieval is an effective defense. In *Advances in Neural Information Processing Systems*, volume 36, 27469–27500.
- Lavergne, T.; Urvoy, T.; and Yvon, F. 2008. Detecting fake content with relative entropy scoring. In *Proceedings of the 2008 International Conference on Uncovering Plagiarism, Authorship and Social Software Misuse*, volume 377, 27–31.
- Liu, Y.; Zhang, H.; Li, C.; Huang, X.; Wang, J.; and Long, M. 2024. Timer: Generative Pre-trained Transformers Are Large Time Series Models. In *Proceedings of the International Conference on Machine Learning*.
- Meister, C.; Wiher, G.; Pimentel, T.; and Cotterell, R. 2022. On the probability–quality paradox in language generation. In *Proceedings of the 60th Annual Meeting of the Association for Computational Linguistics*, 36–45.
- Mitchell, E.; Lee, Y.; Khazatsky, A.; Manning, C. D.; and Finn, C. 2023. DetectGPT: Zero-Shot Machine-Generated Text Detection using Probability Curvature. In *Proceedings of the International Conference on Machine Learning*, volume 202, 24950–24962.
- Nate, G.; Marc, F.; Qiu, S.; and Wilson, A. G. 2023. Large Language Models Are Zero-Shot Time Series Forecasters. In *Advances in Neural Information Processing Systems*.
- Nie, Y.; Nguyen, N. H.; Sinthong, P.; and Kalagnanam, J. 2023. A Time Series Is Worth 64 Words: Long-Term Forecasting with Transformers. In *Proceedings of the International Conference on Learning Representations*.
- Pérez, J.; Barceló, P.; and Marinkovic, J. 2021. Attention Is Turing Complete. *Journal of Machine Learning Research*, 22: 1–35.
- Pu, J.; Sarwar, Z.; Abdullah, S. M.; Rehman, A.; Kim, Y.; Bhattacharya, P.; Javed, M.; and Viswanath, B. 2023. Deepfake Text Detection: Limitations and Opportunities. In *Proc. of IEEE S&P*.
- Pérez, J.; Marinković, J.; and Barceló, P. 2019. On the Turing Completeness of Modern Neural Network Architectures. In *Proceedings of the International Conference on Learning Representations*.
- Radford, A.; Wu, J.; Child, R.; Luan, D.; Amodei, D.; and Sutskever, I. 2019. Language models are unsupervised multitask learners. Technical report, OpenAI.

- Roberts, M.; Hazan, A.; Dittmer, S.; Rudd, J. H. F.; and Schönlieb, C.-B. 2024. The curious case of the test set AUROC. *Nature Machine Intelligence*, 6(4): 373–376.
- Rose, C. S.; and Sesia, A. 2013. Barclays and the LIBOR Scandal. Technical Report 313-075, Harvard Business School.
- Sander, M.; and Peyré, G. 2025. Towards Understanding the Universality of Transformers for Next-Token Prediction. In *International Conference on Representation Learning*, 86901–86920.
- Shi, X.; Wang, S.; Nie, Y.; Li, D.; Ye, Z.; Wen, Q.; and Jin, M. 2025. Time-MoE: Billion-Scale Time Series Foundation Models with Mixture of Experts. In *International Conference on Representation Learning*, volume 2025, 34635–34667.
- Solaiman, I.; Brundage, M.; Clark, J.; Askell, A.; Herbert-Voss, A.; Wu, J.; Radford, A.; and Wang, J. 2019. Release Strategies and the Social Impacts of Language Models. *ArXiv*.
- Su, J.; Zhuo, T. Y.; Wang, D.; and Nakov, P. 2023. DetectLLM: Leveraging Log Rank Information for Zero-Shot Detection of Machine-Generated Text. In *Proceedings of the Conference on Empirical Methods in Natural Language Processing*, 12395–12412.
- Tan, M.; Merrill, M. A.; Gupta, V.; Althoff, T.; and Hartvigsen, T. 2024. Are Language Models Actually Useful for Time Series Forecasting? In *Advances in Neural Information Processing Systems*.
- Tulchinskii, E.; Kuznetsov, K.; Kushnareva, L.; Cherniavskii, D.; Nikolenko, S.; Burnaev, E.; Barannikov, S.; and Piontkovskaya, I. 2023. Intrinsic Dimension Estimation for Robust Detection of AI-Generated Texts. In *Advances in Neural Information Processing Systems*, 39257–39276.
- Uchendu, A.; Le, T.; Shu, K.; and Lee, D. 2020. Authorship Attribution for Neural Text Generation. In *Proceedings of the Conference on Empirical Methods in Natural Language Processing*, 8384–8395.
- Wang, X.; Wang, X.; and Wilkes, M. 2021. *Unsupervised Fraud Detection in Environmental Time Series Data*, 257–277. Springer Singapore.
- Xu, Y.; Wang, Y.; An, H.; Liu, Z.; and Li, Y. 2024. Detecting Subtle Differences between Human and Model Languages Using Spectrum of Relative Likelihood. In *Proceedings of the Conference on Empirical Methods in Natural Language Processing*, 10108–10121.
- Xue, H.; and Salim, F. D. 2023. PromptCast: A New Prompt-Based Learning Paradigm for Time Series Forecasting. *IEEE Transactions on Knowledge and Data Engineering*, 1–14.
- Yang, X.; Cheng, W.; Wu, Y.; Petzold, L. R.; Wang, W. Y.; and Chen, H. 2024. DNA-GPT: Divergent N-Gram Analysis for Training-Free Detection of GPT-Generated Text. In *Proceedings of the International Conference on Learning Representations*.
- Yao, Q.; Yang, C.-H. H.; Jiang, R.; Liang, Y.; Jin, M.; and Pan, S. 2025. Towards Neural Scaling Laws for Time Series Foundation Models. In *Proceedings of the International Conference on Learning Representations*.
- Zhou, T.; Niu, P.; Wang, X.; Sun, L.; and Jin, R. 2023. One Fits All: Power General Time Series Analysis by Pretrained LM. In *Advances in Neural Information Processing Systems*, 43322–43355.

A Definitions

A.1 Time Series and Dataset

We begin by defining the notion of time series throughout this work, and then formalize the dataset constituted by the series.

In classical time series analysis, a time series is typically decomposed into seasonal, trend, and noise components (Box et al. 1978). The seasonal and trend components capture the low-frequency deterministic structure of the series, whereas the noise term accounts for the high-frequency stochastic fluctuations. Henceforth, we merge the seasonal and trend components into a single “trend term”, representing the deterministic and predictable portion of the series, while the noise term captures the unpredictable component.

Definition A.1 (Time Series Decomposition). Given a bounded discrete time series $X_t, t \in \mathbb{Z}$, it can be decomposed into the **Trend Sequence** T_t and the **Noise Process** n_t , formulated as Eq. (4).

$$X_t = T_t + n_t, \quad (4)$$

where T_t is a bounded deterministic sequence such that $\sup_t |T_t| \leq M$, and n_t is an independent Gaussian process with mean 0. We model the variances of n_t by Eq. (5)

$$\sigma_t^2 = \alpha_1 \sigma_{t-1}^2 + \alpha_2 \sigma_{t-2}^2 + \dots + \alpha_l \sigma_{t-l}^2, \quad \sum_{i=1}^l \alpha_i = 1 \quad (5)$$

We first explain the motivation behind the modeling of the variance sequence in Eq. (5). Note the notion of GARCH (Bollerslev 1986), which is formulated by Eq. (6)

$$\sigma_t^2 = \sigma^2 (1 - \alpha - \beta) + \alpha \zeta_{t-1}^2 + \beta \sigma_{t-1}^2, \quad \alpha + \beta < 1. \quad (6)$$

GARCH is motivated by the (exponential) regression of variance to the long-run mean σ after any arbitrary shock ζ_t . Following this rationale and omitting the shock term ζ_t , we replace the “prior variance” σ^2 , which requires prior knowledge of the entire variance sequence, with a “posterior variance” defined by the sample average $\bar{\sigma}_t^2 = \sum_{i=2}^l \alpha'_i \sigma_{t-i}^2$, which is a certain weighted mean of sufficiently long historical variances. Eq. (5) can therefore be reformulated as

$$\sigma_t^2 = \alpha_1 \sigma_{t-1}^2 + (1 - \alpha) \bar{\sigma}_t^2. \quad (7)$$

Note that this decomposition is *unique* as $T_t = \mathbb{E}(X_t)$, $n_t = X_t - T_t$ for all t . In the following analysis, we often relax the Gaussianity of noise and impose the weaker conditions that the distributions are unimodal, symmetric, has well-defined moment and is continuous almost everywhere.

In Definition A.1, we treat the trend and noise of time series as independent components. Building on this, we consider all possible pairings of the trend with all noises. Let the set of T be \mathcal{T} , and denote the set of n_t by N . We have the following definition.

Definition A.2 (Ideal Trend Cluster of T). For a trend sequence T and noise process set N , *Ideal Trend Cluster* of T is defined as Eq. (8).

$$T + N = \{T_t + n_t \mid n_t \in N\}. \quad (8)$$

Intuitively, $T + N$ is the coset of all time series that share the same deterministic trend T but differ in noise n_t .

Based on the separation of trend and noise, we begin from the perspective of trends to analyze which trend sequences can be used to form the dataset for forecasting. In time series forecasting, the model leverages past observations (and its internal state) to predict future values. Wold’s decomposition theory shows that the exact prediction of predictable (trend) components requires infinite past information (Box et al. 1978), and in practical forecasting, this is approximated by leveraging sufficiently long finite histories. Consequently, at the trend level, the forecast must be a deterministic function of the same history: identical historical inputs cannot produce different trend predictions (Box et al. 1978). This implies that each distinct trend must correspond to an infinite unique history, and we formalize this distinction in Definition A.3.

Definition A.3 (Distinct Trends). For trend sequences T_t, T'_t , if for all $\tau \in \mathbb{Z}$ there exists $s \leq \tau$ such that $T_s \neq T'_s$, then T_t and T'_t are **distinct**. Otherwise, T_t and T'_t are **historically equivalent**, denoted as $T_t \sim_H T'_t$.

This indicates that for two distinct trends T_t, T'_t , there is no minimal s such that $T_t = T'_t$ for all $t \leq s$. The relations defined in Definition A.3 allow us to partition the trend set \mathcal{T} , enabling the construction of an “ideal dataset” whose trend sequences are mutually distinct.

The historical equivalence relationship, by definition, satisfies reflexivity, symmetry, and transitivity and is an equivalence relationship in the trend set. Consequently, it partitions the trend set into disjoint equivalence classes.

$$\mathcal{T} / \sim_H = \{[T] \mid T \in \mathcal{T}\}, \quad [T] = \{T' \mid T' \sim_H T\}, \quad (9)$$

where $\bigcup_{[T] \in \mathcal{T} / \sim_H} [T] = \mathcal{T}$, $[T] \cap [T'] = \emptyset$ if $[T] \neq [T']$. Note that any two trends in different equivalence classes are distinct. According to the **Axiom of Choice**, we select any representative element from each equivalence class to obtain a **maximally distinct set**, and use it to construct the **ideal dataset**.

Definition A.4 (Ideal Dataset). A set $S \subseteq \mathcal{T}$ is **maximally distinct** if

1. (Pairwise distinct) $\forall T_1, T_2 \in S, T_1 \neq T_2 \Rightarrow T_1$ and T_2 are distinct;
2. (Maximality) $\forall T \in \mathcal{T}, \exists T' \in S$ s.t. $T \sim_H T'$.

The set of ideal trend clusters for all trend sequences in a *maximally distinct set* S is an **Ideal Dataset**, which is formulated as Eq. (10)

$$D = \{T + N \mid T_t \in S\}. \quad (10)$$

In the construction of the maximally distinct set and ideal dataset, we choose representative elements from an uncountably infinite family of non-empty equivalence classes. Although this construction is non-constructive and not unique, the theoretical existence is guaranteed according to the Axiom of Choice. Notably, for any two maximally distinct sets S_1 and S_2 , we have $\forall T_t^{(1)} \in S_1 \exists T_t^{(2)} \in S_2$ such that $T_t^{(1)} \sim_H T_t^{(2)}$. This indicates that the maximally distinct set is *unique* modulo the equivalence relation \sim_H .

Given the dataset of intrinsically distinct time series defined above, we next introduce the set of sufficiently long historical sequences used for forecasting.

Definition A.5 (History Set). Let H be the minimal length of the forecast history. Given an ideal dataset D , we define the k -**history set** ($k \geq H$) as Eq. (11).

$$\text{HS}_k = \{\mathbf{X}_{-k:0} \mid X_t \in D\}. \quad (11)$$

Notably, since $X_t = T_t + n_t$, we have that any two distinct histories in HS_k differ in either trend or noise component. The **history set** of an ideal dataset D is defined as

$$\text{HS} = \bigcup_{k \geq H} \text{HS}_k. \quad (12)$$

We first note that choosing 0 as the historical end point is without loss of generality. For any $\mathbf{X}_{-k+s:s}$, it can be mapped to $\mathbf{X}'_{-k:0}$, and therefore we have $\{\mathbf{X}_{-k+s:s} \mid X_t \in D\} = \{\mathbf{X}_{-k:0} \mid X_t \in D\}, \forall s$. For notational consistency, we fix the historical end point as 0.

Intuitively, the history set HS contains all sufficiently long distinct sub-series. Given any history $\mathbf{X}_{-k:0} \in \text{HS}_k$, once a one-step forecast X_1 is predicted and appended, we obtain a new history $\mathbf{X}_{-k:1} \in \text{HS}_{k+1}$, thus enabling recursive forecasting over arbitrary horizons.

A.2 Ideal Model and Loss

In this section, we introduce the concept of ideal model for time series forecasting. In the forecasting task, a model takes a sufficiently long history as input and generates the model's *internal probability distribution* to sample prediction values. For the Large Time Series Models that sample real values at equal intervals into discrete set, formulated as Eq. (13)

$$\mathcal{V} = \{v_i \mid v_{i+1} - v_i = \Delta, -R \leq v_i \leq R\}, \quad (13)$$

the internal distributions are presented by a discrete probability mass function p_θ over \mathcal{V} . More concretely, given any history $\mathbf{X}_{-H:t-1} \in \text{HS}$, the internal probability distribution is $p_{\theta,\Delta}(z_t \mid \mathbf{X}_{-H:t-1})$. In the limit $R \rightarrow \infty$, \mathcal{V} extends to a countably infinite discretization of \mathbb{R} . We denote \mathcal{V} as the *vocabulary* and each $v \in \mathcal{V}$ is a token, which represents an interval $[v - \frac{\Delta}{2}, v + \frac{\Delta}{2})$. We consider our forecasting models and the internal probability distributions over this extended vocabulary.

Formally, we measure the discrepancy between the true next-step outcome and the model's internal distribution using cross-entropy. In the following section, we will demonstrate that if losses such as MSE are used, we immediately draw the conclusion of uncertainty convergence, and therefore the selection of cross-entropy is without loss of generality. With fixed Δ , we first propose the loss function for model training.

Definition A.6 (Δ -Loss Function). Given history $\mathbf{X}_{-H:0}$ and a fixed forecast length τ , the Δ -**Loss Function** of forecast \mathbf{X}_τ is formulated as Eq. (14).

$$\mathcal{L}_{\theta,\Delta}(\mathbf{X}_\tau) = \sum_{i=1}^{\tau} -\log p_{\theta,\Delta}(z_i = X_i \mid \mathbf{X}_{-H:i-1}). \quad (14)$$

It should be noted that, given the stochastic process nature of X_t , $\mathcal{L}_{\theta,\Delta}(\mathbf{X}_\tau)$ is a *random variable* dependent on \mathbf{X}_τ .

Note that for any two time points $i \neq j$, the internal distributions $p_{\theta,\Delta}(z_i \mid \mathbf{X}_{-H:i-1})$ and $p_{\theta,\Delta}(z_j \mid \mathbf{X}_{-H:j-1})$ are independent if their histories are given. Consequently, the loss in Definition A.6 decomposes into a sum of mutually independent per-step losses as Eq. (15), and the global loss $\mathcal{L}_{\theta,\Delta}$ can be minimized by minimizing each $\ell_{\theta,\Delta}(X_i)$.

$$\ell_{\theta,\Delta}(X_i) = -\log p_{\theta,\Delta}(z_i = X_i \mid \mathbf{X}_{-H:i-1}). \quad (15)$$

Based on the loss in Definition A.6, we define the discrete ideal model.

Definition A.7 (Δ -Ideal Model). For any finite time series segment \mathbf{X}_τ of any ideal trend cluster in the ideal dataset, the mathematical expectation of the Δ -loss function is minimal for the Δ -**Ideal Model**.

$$\theta = \arg \min_{\theta} \mathbb{E}(\mathcal{L}_{\theta,\Delta}(\mathbf{X}_\tau)), \forall X \in C(T), \forall C(T) \in D. \quad (16)$$

We assume the existence of such models, which is discussed in the following paragraphs. We first demonstrate the following property of the Δ -ideal model.

Theorem A.8. Let $p_{\theta,\Delta}(z_t)$ denote the Δ -ideal model's internal probability distribution with history $\mathbf{X}_{-H:t-1}$, and denote the probability density function of X_t to be f_t , we have

$$p_{\theta,\Delta}(z_t = v) = \int_{v - \frac{\Delta}{2}}^{v + \frac{\Delta}{2}} f_t(z) dz. \quad (17)$$

Let $f_{\theta,\Delta} = \frac{p_{\theta,\Delta}(z_t)}{\Delta}$, we have when $\Delta \rightarrow 0$,

$$f_{\theta,\Delta} \rightarrow f_t \text{ a.e.} \quad (18)$$

The proof is given in Section B.1.

Theorem A.8 indicates that the Δ -ideal model achieves a perfect prediction of the original time series with granularity Δ . More precisely, the probability mass function of the internal distribution, by endowing the probability of each token v to the corresponding interval $[v - \frac{\Delta}{2}, v + \frac{\Delta}{2})$, is a simple-function approximation of f_t with granularity Δ , and as $\Delta \rightarrow 0$ it converges to f_t in the sense of measures.

On the other hand, as $\Delta \rightarrow 0$, the vocabulary \mathcal{V} converges to \mathbb{R} in the sense of Hausdorff metric. We now turn to the development of a continuous ideal model and its corresponding loss, and proceed to verify that this "limit model" is exactly the limit of Δ -ideal model.

Definition A.9 (Loss Function). Let $f_\theta(z_t \mid \mathbf{X}_{-H:t-1})$ be the probability density function of the internal probability distribution given $\mathbf{X}_{-H:t-1}$, the **Loss Function** is formulated as Eq. (19).

$$\mathcal{L}_\theta(\mathbf{X}_\tau) = \sum_{i=1}^{\tau} -\log f_\theta(z_i = X_i \mid \mathbf{X}_{-H:i-1}). \quad (19)$$

Notably, the loss function is not the point-wise limit of Δ -loss function. Instead, it emerges through the limit of its normalized form, as shown in Eq. (20)

$$\lim_{\Delta \rightarrow 0} \sum_{i=1}^{\tau} -\log \frac{p_{\theta,\Delta}(z_i = X_i \mid \mathbf{X}_{-H:i-1})}{\Delta} = \mathcal{L}_\theta(\mathbf{X}_\tau). \quad (20)$$

With fixed Δ the left hand side of Eq. (20) is minimized in expectation simultaneously with Δ -loss function. Therefore, the loss function in Definition A.9 can be regarded as the “limit” of Δ -loss function.

Similarly to Definition A.6, $\mathcal{L}_\theta(\mathbf{X}_\tau)$ is also a *random variable*, and the loss alike can be minimized at each step.

Definition A.10 (Ideal Model). For any finite time series segment \mathbf{X}_τ of any ideal trend cluster in the ideal dataset, the mathematical expectation of the loss function is minimal for the **Ideal Model**.

$$\theta = \arg \min_{\theta} \mathbb{E}(\mathcal{L}_\theta(\mathbf{X}_\tau)), \forall X \in C(T), \forall C(T) \in D. \quad (21)$$

Assuming the existence of the ideal model, we show that it satisfies the following property. We show that the ideal model *can* be regarded as a “limit model” of the Δ -ideal model in terms of internal probability distribution.

Theorem A.11. Let $f_\theta(z_t)$ denote the ideal model’s internal probability distribution with history $\mathbf{X}_{-H:t-1}$, and denote the probability density function of X_t to be f_t , we have

$$f_\theta(z_t) \equiv f_t, \text{ a.e.} \quad (22)$$

The proof is given in Section B.1. Theorem A.11 establishes that the internal distribution of ideal model coincides almost everywhere with the true probability distribution, which is exactly the limit distribution of Δ -ideal models when $\Delta \rightarrow 0$. This indicates that the ideal model is exactly the “limit model” of Δ -ideal model, and the definition is well-defined.

On the other hand, Theorem A.11 shows that, given history $\mathbf{X}_{-H:t-1}$ the ideal model can recover the true probability distribution, indicating the computability of σ_t^2 . Since it follows Eq. (5), we conclude that the model has internalized this variance recursion.

A.3 Model Evaluation Function

In practice, once a forecasting model produces a candidate sequence $\hat{\mathbf{X}}_\tau$, we need a principled way to assess its accuracy against the true sequence \mathbf{X}_τ , which measure the “distance” between $\hat{\mathbf{X}}_\tau$ and \mathbf{X}_τ . The notion of distance is grounded in the ℓ_p norm in finite dimensions, and drawing inspiration from MAE and MSE, we introduce a positive monotonic function to regulate the error. We formalize the aforementioned concepts and generalize them as Definition A.12.

Definition A.12 (Model Evaluation Function). For any finite time series segment \mathbf{X}_τ of any ideal trend cluster in the Ideal Dataset, and its corresponding forecast series $\hat{\mathbf{X}}_\tau$, the **evaluation function** is formulated as Eq. (23).

$$\text{Eva} = \left[\sum_{i=1}^{\tau} g(|X_i - \hat{X}_i|^p) \right]^{\frac{1}{p}}, \quad (23)$$

where g is a monotonically increasing non-negative function and $p \in [1, +\infty]$.

Definition A.12 introduces a general form of evaluation function that encompasses common metrics such as MAE and MSE. When g is a positive proportional function, that is, $g(x) = \alpha x, \alpha > 0$, the evaluation function is proportional to the norm ℓ_p .

A.4 Theoretical Existence of Ideal Model

The perfect prediction property of ideal model, shown in Theorem A.11, provides another view of the ideal model, and reduces the problem of loss minimization over all time series to the identification of each single deterministic function.

We first demonstrate that the ideal model, which is a mapping from sequences to distribution, can potentially be an injection, inferring that no two distinct input sequences are forced to produce the same distribution. The length of history is arbitrary as $k \geq H$, and the histories therefore constitute a set $\bigcup_{H \geq L} \mathbb{R}^H$. On the other hand, since the probability density is continuous almost everywhere, it is completely determined by its values on a countable dense subset of \mathbb{R} , and the space of such distributions can be identified with $\mathbb{R}^{\mathbb{N}}$. The ideal model is therefore the function $f : \bigcup_{H \geq L} \mathbb{R}^H \rightarrow \mathbb{R}^{\mathbb{N}}$. According to the Cantor-Bernstein theorem, we have

$$\text{Card} \left(\bigcup_{H \geq L} \mathbb{R}^H \right) = \text{Card}(\mathbb{R}^{\mathbb{N}}), \quad (24)$$

which provides the prerequisite for the injection condition.

We next provide that, at any prescribed precision, the ideal model’s mapping f is Type-2 computable. Moreover, every finite-term approximation of f (e.g., simple function approximation) is computable, and is applied in real-world model applications. Since sequence modeling architectures such as RNNs (Chung and Siegelmann 2021; Pérez, Marinković, and Barceló 2019) and Transformers (Sander and Peyré 2025; Pérez, Barceló, and Marinkovic 2021) are Turing-complete and can approximate any computable or Type-2 computable functions with infinite memory, runtime and arbitrary precision. This indicates the theoretical existence of the ideal model.

B Theoretical Analysis of Contraction Hypothesis

In Section 4.2, we provided a qualitative outline of the proof strategy for the Contraction Hypothesis. In this section, we formally state this hypothesis and provide the proofs of all critical propositions.

B.1 Distributional Consistency

In Definition A.10 and Theorem A.11, we propose the concept of ideal model and generalize that it makes distribution-perfect predictions given histories. The concept of ideal model derives directly from its discrete form (see Definition A.7) with a corresponding property (see Theorem A.8). We now prove the properties of the ideal models in both discrete and continuous scenarios.

Theorem A.8. Let $p_{\theta,\Delta}(z_t)$ denote the Δ -ideal model's internal probability distribution with history $\mathbf{X}_{-H:t-1}$, and denote the probability density function of X_t to be f_t , we have

$$p_{\theta,\Delta}(z_t = v) = \int_{v-\frac{\Delta}{2}}^{v+\frac{\Delta}{2}} f_t(z) dz. \quad (17)$$

Let $f_{\theta,\Delta} = \frac{p_{\theta,\Delta}(z_t)}{\Delta}$, we have when $\Delta \rightarrow 0$,

$$f_{\theta,\Delta} \rightarrow f_t \text{ a.e.} \quad (18)$$

Proof of Theorem A.8. We begin from a lemma.

Lemma B.1. Given positive integer $n \geq 1$ and fixed positive reals a_1, \dots, a_n such that $\sum_{i=1}^n a_i = 1$, for positive reals b_1, \dots, b_n such that $\sum_{i=1}^n b_i = 1$, the following equation holds:

$$\sum_{i=1}^n a_i \ln b_i \leq \sum_{i=1}^n a_i \ln a_i, \quad (25)$$

and equation holds if and only if $a_i = b_i, \forall i$.

Proof of Lemma B.1. Under the constraint of $\sum_{i=1}^n b_i = 1$, the Lagrange function is formulated as follows:

$$L = \sum_{i=1}^n a_i \ln b_i - \lambda \left(\sum_{i=1}^n b_i - 1 \right). \quad (26)$$

The partial derivatives of the function are

$$\frac{\partial L}{\partial b_i} = \frac{a_i}{b_i} - \lambda, \quad \frac{\partial^2 L}{\partial b_i^2} = -\frac{a_i}{b_i^2}, \quad \frac{\partial^2 L}{\partial b_i \partial b_j} = 0, \quad i \neq j, \quad (27)$$

and the extremum condition is satisfied when $\frac{a_i}{b_i} = \lambda$. According to the constraint, we have $\lambda = 1, a_i = b_i$. At this point, the Hessian matrix is negative definite, indicating that a local maximum is obtained.

Due to the strict concavity of the logarithmic function, it follows that L is strictly concave and therefore the maximum value is achieved at the local maximum. \square

We have

$$\begin{aligned} \mathbb{E}(\mathcal{L}) &= \sum_{v \in \mathcal{V}} P \left\{ v - \frac{\Delta}{2} \leq X_i \leq v + \frac{\Delta}{2} \right\} (-\log p_{\theta,\Delta}(z_i = v)) \\ &= \sum_{v \in \mathcal{V}} \int_{v-\frac{\Delta}{2}}^{v+\frac{\Delta}{2}} f_t(z) dz (-\log p_{\theta,\Delta}(z_i = v)). \end{aligned} \quad (28)$$

According to Lemma B.1, the expectation is minimized when

$$p_{\theta,\Delta}(z_t = v) = \int_{v-\frac{\Delta}{2}}^{v+\frac{\Delta}{2}} f_t(z) dz$$

holds for all $v \in \mathcal{V}$. Notably, we have $f_{\theta,\Delta}$ is measurable for all $\Delta > 0$ and f_t is measurable. According to Lebesgue differential theorem, we have

$$\lim_{\Delta \rightarrow 0} f_{\theta,\Delta}(v) = \lim_{\Delta \rightarrow 0} \frac{1}{\Delta} \int_{v-\frac{\Delta}{2}}^{v+\frac{\Delta}{2}} f_t(z) dz = f_t(v)$$

for almost every $v \in \mathbb{R}$. \square

Theorem A.11. Let $f_{\theta}(z_t)$ denote the ideal model's internal probability distribution with history $\mathbf{X}_{-H:t-1}$, and denote the probability density function of X_t to be f_t , we have

$$f_{\theta}(z_t) \equiv f_t, \text{ a.e.} \quad (22)$$

Proof of Theorem A.11. We begin with a lemma.

Lemma B.2. Let f be a fixed positive measurable function such that $\int_{-\infty}^{\infty} f(x) dx = 1$. For a positive measurable function g such that $\int_{-\infty}^{\infty} g(x) dx = 1$, then the following equation holds:

$$\int_{-\infty}^{\infty} f(x) \ln g(x) dx \leq \int_{-\infty}^{\infty} f(x) \ln f(x) dx.$$

The maximum value occurs if and only if $f = g$ almost everywhere.

Proof of Lemma B.2. We construct the Lagrange functional as follows:

$$L(g) = \int_{-\infty}^{\infty} f(x) \ln g(x) dx - \lambda \left(\int_{-\infty}^{\infty} g(x) dx - 1 \right)$$

The variations of this functional are

$$\begin{aligned} \delta L(g) &= \int_{-\infty}^{\infty} \left(\frac{f(x)}{g(x)} - \lambda \right) \delta b(x) dx, \\ \delta^2 L(g) &= \int_{-\infty}^{\infty} -\frac{f(x)}{g(x)^2} (\delta b(x))^2 dx. \end{aligned} \quad (29)$$

The functional extremum condition holds when $\delta L(g) = 0, \forall b$, indicating $\frac{f(x)}{g(x)} - \lambda = 0$ almost everywhere. According to the constraint, we have $\lambda = 1$, and $f(x) = g(x)$ holds almost everywhere. At this point, the second variation is always less than 0, indicating a local maximum.

Note that for any positive measurable function g_1, g_2 and any $\alpha \in [0, 1]$, we have

$$\begin{aligned} &L(\alpha g_1(x) + (1 - \alpha)g_2(x)) \\ &= \int_{-\infty}^{\infty} f(x) \ln(\alpha g_1(x) + (1 - \alpha)g_2(x)) dx \\ &\leq \int_{-\infty}^{\infty} \alpha f(x) \ln g_1(x) + f(x)(1 - \alpha) \ln g_2(x) dx \\ &= \alpha L(g_1(x)) + (1 - \alpha)L(g_2(x)). \end{aligned}$$

Thus, the functional L is concave and the maximum value is obtained when $f = g$ holds almost everywhere. \square

For any time series, we have

$$\mathbb{E}(\mathcal{L}) = - \int_{-\infty}^{\infty} f_t(v) \log f_{\theta}(z_t = v) dv \quad (30)$$

According to Lemma B.2, the expectation of loss is minimized when $f_{\theta} = f_t$ holds almost everywhere. \square

Specifically, we propose a corollary of Theorem A.11 (see Corollary 4.2) that if the true sequence is entirely deterministic (i.e., has zero uncertainty), ideal models make value-perfect predictions.

Corollary 4.2. If $\sigma_t^2 = 0$, we have $f_\theta(z = v) = \delta(v - T_t)$, where δ is the Dirac- δ function.

Proof of Corollary 4.2. Corollary 4.2 is a special case of Lemma 4.1 where $f_t = \delta$. In this proof, we analyze the discrete form, as the continuous ideal model is the limit of the discrete Δ -ideal model.

According to Chebyshev's inequality $P\{X_t = T_t\} = 1$. We calculate the loss in this time point.

$$\begin{aligned} \mathbb{E}(\mathcal{L}(X_t)) &= \sum_{v \in \mathcal{V}} P\{X_t = v\} \cdot (-\log p_\theta(z_t = v)) \\ &= -\log p_\theta(z_t = T_t) \geq 0 \end{aligned} \quad (31)$$

According to Lemma B.1, the equation holds if and only if $\arg \max_v p_\theta(z_t = v) = T_t, p_\theta(z_t = T_t) = 1$, with minimal loss expectation. \square

B.2 Sampling-Induced Variance Scaling

When given any history $\mathbf{X}_{-H:t-1}$ to predict \hat{X}_t , TSLMs utilize the internal probability distributions f_θ to obtain the sampling distributions \hat{f}_t . The modification of f_θ derives from sampling strategies, including scaling and symmetric truncation. We first prove the following property of the strategies.

Theorem B.3. *The sampling strategies preserves the expectation of f_θ .*

Proof of Theorem B.3. Denoting $\int_{-\infty}^{\infty} f(z) dz = E_z$. For any symmetric probability density function f over \mathbb{R} , the scaling transformation can be formulated by Eq. (32)

$$f_T(z) = \frac{f(z)^{\frac{1}{T}}}{\int_{-\infty}^{\infty} f(z)^{\frac{1}{T}} dz}. \quad (32)$$

Since $f(E+z) = f(E-z)$ holds for all $z \in \mathbb{R}$, we therefore have

$$\begin{aligned} &\int_{-\infty}^{\infty} \frac{zf(z)^{\frac{1}{T}}}{\int_{-\infty}^{\infty} f(x)^{\frac{1}{T}} dx} dz \\ &= \frac{\int_{-\infty}^{\infty} E_z f(z)^{\frac{1}{T}} + \int_{-\infty}^{\infty} (z - E_z) f(z)^{\frac{1}{T}}}{\int_{-\infty}^{\infty} f(x)^{\frac{1}{T}} dx} = E_z. \end{aligned} \quad (33)$$

The symmetric truncation can be formulated by

$$f_a(z) = \begin{cases} \frac{f(z)}{\int_{E_z-a}^{E_z+a} f(x) dx}, & E_z - a \leq z \leq E_z + a; \\ 0, & \text{otherwise.} \end{cases} \quad (34)$$

We have

$$\int_{-\infty}^{\infty} z f_a(z) dz = \int_{E_z-a}^{E_z+a} \frac{zf(z)}{\int_{E_z-a}^{E_z+a} f(x) dx} = E_z. \quad (35)$$

\square

Denoting the uncertainty modification of the sampling strategies from internal distribution variance $\tilde{\sigma}_t^2$ to sampling distribution variance $\hat{\sigma}_t^2$ as

$$\hat{\sigma}_t^2 = \gamma_t \cdot \tilde{\sigma}_t^2, \quad (36)$$

and in recursive forecasting we have

Theorem B.4. *Given history $\mathbf{X}_{-H:0}$, we have that for any $\tau > 0$, there is*

$$\mathbb{E}(\hat{X}_t) = T_t, \forall 1 \leq t \leq \tau. \quad (37)$$

Proof of Theorem B.4. We define $\hat{X}_0 = X_0$ as they share the same history. For the forecast of \hat{X}_1 with $\mathbf{X}_{-H:0}$, we have $\int_{-\infty}^{\infty} f_\theta(z_1) dz_1 = \int_{-\infty}^{\infty} f_1(z) dz = T_1$ due to Lemma 4.1. According to Theorem B.3, we have

$$\mathbb{E}(\hat{X}_1) = \int_{-\infty}^{\infty} f_\theta(z_1) dz_1 = T_1. \quad (38)$$

Given that $\mathbb{E}(\hat{X}_t) = T_t$ holds for all $t \leq s-1$, we have that with history $\mathbf{X}_{-H:0}, \hat{\mathbf{X}}_{\tau-1}$. With knowledge of this and according to Lemma 4.1, the internal probability distribution at time τ is of expectation T_τ . According to Theorem B.3, we have

$$\mathbb{E}(\hat{X}_\tau) = \int_{-\infty}^{\infty} f_\theta(z_\tau) dz_\tau = T_\tau. \quad (39)$$

By induction, Eq. (39) holds for all $1 \leq t \leq \tau$ for all possible τ . \square

Given the trend-perfect forecast for arbitrary sampling strategies or γ_t selection, we show that when f_θ is fixed, the modification γ_t influences the forecast and its evaluation.

Lemma 4.3. *The expectation of the model evaluation function $\mathbb{E}(\text{Eva})$ increases monotonically with respect to all $\hat{\sigma}_t$.*

Proof of Lemma 4.3. Let $Z_t = X_t - \hat{X}_t \sim \mathcal{N}(0, \sigma_t^2 + \hat{\sigma}_t^2)$. We begin by presenting a definition and its associated properties.

Definition B.5 (First-Order Stochastic Dominance). For variables z^1 and z^2 , if

$$P\{|z^1| \geq z\} \leq P\{|z^2| \geq z\}, \forall z \in \mathbb{R}, \quad (40)$$

then z^2 **first-order stochastically dominates** z^1 , denoted by $z^1 \leq_{st} z^2$

Lemma B.6 (Gaussian First-Order Stochastic Dominance). *For variables $z^1 \sim \mathcal{N}(0, \sigma_1^2)$ and $z^2 \sim \mathcal{N}(0, \sigma_2^2)$, if $\sigma_1^2 \leq \sigma_2^2$, then $|z^1| \leq_{st} |z^2|$.*

Proof of Lemma B.6. Given two Gaussian variables z^1, z^2 with their corresponding folded normal variables $|z^1|, |z^2|$ and probability distributions $f_{|z^1|}, f_{|z^2|}$. Since

$$\begin{aligned} P\{|z^1| \geq z\} &= 2 \left[1 - \Phi\left(\frac{z}{\sigma_1}\right) \right] = \frac{2}{\sqrt{\pi}} \int_{\frac{z}{\sqrt{2}\sigma_1}}^{\infty} e^{-t^2} dt, \\ P\{|z^2| \geq z\} &= \frac{2}{\sqrt{\pi}} \int_{\frac{z}{\sqrt{2}\sigma_2}}^{\infty} e^{-t^2} dt, \end{aligned} \quad (41)$$

holds for all z , we have $P\{|z^1| \geq z\} \leq P\{|z^2| \geq z\}$ for all z . This indicates that $|z^1| \leq_{st} |z^2|$. \square

Lemma B.7 (Preservation under Monotonic Transformations). *For a monotonically increasing function g and variables z^1 and z^2 , if $z^1 \leq_{st} z^2$, then $g(z^1) \leq_{st} g(z^2)$.*

Proof of Lemma B.7. For all z , we have

$$\begin{aligned} P\{g(z^1) \geq z\} &= P\{z^1 \geq g^{-1}(z)\} \\ &\leq P\{z^2 \geq g^{-1}(z)\} = P\{g(z^2) \geq z\}, \end{aligned} \quad (42)$$

indicating $g(z^1) \leq_{st} g(z^2)$. Notably, here g^{-1} is the *generalized inverse* defined as

$$g^{-1}(y) = \inf\{x \mid g(x) \leq y\}. \quad (43)$$

□

Lemma B.8 (Additivity over Independent Variables). *For variables z^1, z^2 and z^3 , if $z^1 \leq_{st} z^2$ and z^1, z^2 are independent of z^3 , then $z^1 + z^3 \leq_{st} z^2 + z^3$.*

Proof of Lemma B.8. For all z , we have

$$\begin{aligned} P\{z^1 + z^3 \geq z\} &= \int P\{z^1 \geq z - v\} dF_{z^3}(v) \\ &\leq \int P\{z^2 \geq z - v\} dF_{z^3}(v) = P\{z^2 + z^3 \geq z\}, \end{aligned} \quad (44)$$

indicating $z^1 + z^3 \leq_{st} z^2 + z^3$. □

Lemma B.9 (Expectation Dominance over Utility). *For variables z^1 and z^2 , if $z^1 \leq_{st} z^2$, then for every monotonically increasing function u , we have*

$$\mathbb{E}(u(z^1)) \leq \mathbb{E}(u(z^2)) \quad (45)$$

if both expectations exist.

Proof of Lemma B.9. Let

$$u^+(z) = \max\{u(z), 0\}, \quad u^-(z) = \max\{-u(z), 0\},$$

therefore $u = u^+ - u^-$ with both $u^+, u^- \geq 0$ and $u^+, -u^-$ increasing monotonically. If and only if $\mathbb{E}(|u(z)|)$ exists, $\mathbb{E}(u(z))$ exists with

$$\mathbb{E}(u(z)) = \mathbb{E}(u(z^+)) - \mathbb{E}(u(z^-))$$

potentially for $z = z^1$ or $z = z^2$. Therefore, without loss of generality, let $u(z) \geq 0$ (because for u^- there is a similar conclusion).

Therefore, for non-negative variables $u(z^1), u(z^2)$, we have

$$\begin{aligned} \mathbb{E}(u(z^1)) &= \int_0^\infty P\{u(z^1) \geq u\} du, \\ \mathbb{E}(u(z^2)) &= \int_0^\infty P\{u(z^2) \geq u\} du. \end{aligned} \quad (46)$$

Given $z^1 \leq_{st} z^2$ and according to Lemma B.7, we have $u(z^1) \leq_{st} u(z^2)$, indicating $P\{u(z^1) \geq u\} \leq P\{u(z^2) \geq u\}, \forall u > 0$. Therefore,

$$\begin{aligned} \mathbb{E}(u(z^1)) - \mathbb{E}(u(z^2)) &= \int_0^\infty P\{u(z^1) \geq u\} - P\{u(z^2) \geq u\} du \leq 0. \end{aligned} \quad (47)$$

□

Given the real time series segment \mathbf{X}_τ and any forecast series $\hat{\mathbf{X}}_\tau$, we define $\mathbf{Z}_\tau = \mathbf{X}_\tau - \hat{\mathbf{X}}_\tau$ where each $Z_t \sim \mathcal{N}(0, \sigma_t^2 + \hat{\sigma}_t^2)$ is independently distributed. With an arbitrary choice of $1 \leq i \leq \tau$, we consider a varying variance of Z_i and set all other variances of $Z_i (t \neq i)$ fixed. We define $Z := \sum_{j \neq i} g(|Z_j|^p)$, which is independent from Z_i . If it is replaced by $Z'_i \sim \mathcal{N}(0, \sigma_t^2 + \hat{\sigma}_t'^2)$ such that $\hat{\sigma}_t'^2 \geq \hat{\sigma}_t^2$, according to Lemma B.6 we have $|Z_i| \leq_{st} |Z'_i|$. According to Lemma B.7, we have $g(|Z_i|^p) \leq_{st} g(|Z'_i|^p)$. According to Lemma B.8, we have

$$\begin{aligned} \sum_{j=1}^\tau g\left(|X_j - \hat{X}_j|^p\right) &= g(|Z_i|^p) + \sum_{j \neq i} g(|Z_j|^p) \\ &= g(|Z_i|^p) + Z \leq_{st} g(|Z'_i|^p) + Z \\ &= g(|Z'_i|^p) + \sum_{j \neq i} g(|Z_j|^p). \end{aligned} \quad (48)$$

According to Lemma B.9 and let $u(z) = z^{\frac{1}{p}}$, we have

$$\begin{aligned} \mathbb{E}\left(\left[\sum_{j=1}^\tau g(|Z_j|^p)\right]^{\frac{1}{p}}\right) &= \mathbb{E}\left(\left[g(|Z_i|^p) + \sum_{j \neq i} g(|Z_j|^p)\right]^{\frac{1}{p}}\right). \end{aligned} \quad (49)$$

This indicates that for all $1 \leq i \leq \tau$, we have $\mathbb{E}(\text{Eva})$ is monotonically increasing in $\hat{\sigma}_t^2$. □

Notably, we draw a corollary from Lemma 4.3 that, if metrics such as MSE are used as training loss, the conclusion of uncertainty convergence is immediate.

Corollary B.10. *If the loss function is defined as the model evaluation function Eva , which is*

$$\mathcal{L} = \left[\sum_{i=1}^\tau g(|X_i - z_i|^p)\right]^{\frac{1}{p}}, \quad (50)$$

we have

$$f_\theta(z = v) = \delta(v - T_t) \quad (51)$$

for all $\sigma^2 \geq 0$.

Proof of Corollary B.10. According to Lemma 4.3, the expectation of \mathcal{L} is monotonically increasing in the variance of $X_i - z_i$, it is minimized if and only if $\hat{\sigma}_t^2 = 0$ for all i and the expectation to be T_t , and therefore we obtain that

$$f_\theta(z = v) = \delta(v - T_t), \text{ a.e.} \quad (52)$$

□

Since $\hat{\sigma}_t^2 = \gamma_t \tilde{\sigma}_t^2 = \gamma_t \sigma_t^2$, we have that the lower each γ_t , the lower the model evaluation function's value, indicating better performance. Typically, $\gamma_t < 1$ is universally adopted (e.g., lowering temperature) at each time t .

B.3 Recursive Variance Reduction

Building on the intuition of γ_t , we further analyze the variance evolution in the process of forecasting. According to Lemma 4.1, the ideal model reproduces any distribution with variance satisfying $\sigma_t^2 = \sum_{i=1}^l \alpha_i \sigma_{t-i}^2$. When the forecasts $\hat{X}_1, \hat{X}_2, \dots$ are fed back as histories, their variances $\hat{\sigma}_1^2, \hat{\sigma}_2^2, \dots$ involve in this recurrence, and we have Eq. (53).

$$\tilde{\sigma}_t^2 = \sum_{i=1}^l \alpha_i \hat{\sigma}_{t-i}^2 = \sum_{i=1}^l \alpha_i \gamma_{t-i} \tilde{\sigma}_{t-i}^2, \quad \sum_{i=1}^l \alpha_i = 1. \quad (53)$$

If $\gamma_t \leq q < 1$ holds for all t , we consider the linear recurrence sequence defined by

$$\tilde{\sigma}_t^2 \leq \sum_{i=1}^l q \alpha_i \tilde{\sigma}_{t-i}^2, \quad (54)$$

whose general term can be written by

$$\tilde{\sigma}_t^2 = P_1 r_1^t + P_2 r_2^t + \dots + P_j r_j^t, \quad (55)$$

where r_1, \dots, r_j are distinct roots of the characteristic polynomial and $\deg(P_1) + 1, \dots, \deg(P_j) + 1$ are their respective multiplicities. Given Eq. (55), we draw the following conclusion.

Theorem B.11. $|r_i| < 1$ holds for all $1 \leq i \leq l$.

Proof of Theorem B.11. Since r_i is the root of the characteristic polynomial

$$r^l - \sum_{i=1}^l q \alpha_i r^{l-i}, \quad (56)$$

if there exists i such that $|r_k| \geq 1$, we have

$$\begin{aligned} |r_k|^l &= \left| \sum_{i=1}^l q \alpha_i r_k^{l-i} \right| \leq \sum_{i=1}^l q \alpha_i |r_k|^{l-i} = \sum_{i=1}^l q \alpha_i |r_k|^{-i} \\ &\leq |r_k|^l \sum_{i=1}^l q \alpha_i < |r_k|^l, \end{aligned} \quad (57)$$

which leads to a contradiction, thereby confirming the original conclusion. \square

According to Eq. (55), we have that when $t \rightarrow \infty$, $\tilde{\sigma}_t^2$ converges to 0. By contrast, when $\gamma_t \geq q > 1$ holds for all t , we have the opposite conclusion that $\exists i$ such that $|r_i| > 1$ and $\tilde{\sigma}_t^2$ diverges to infinity.

When $\gamma_t \equiv 1$, we have Eq. (53) to be reformulated by

$$\tilde{\sigma}_t^2 = C_1 \cdot 1 + P_2 r_2^t + \dots + P_j r_j^t, \quad (58)$$

indicating that 1 is a simple root of the characteristic equation. Similarly to Theorem B.11, we have $|r_i| \leq 1$ for all $2 \leq i \leq j$. Therefore, $\tilde{\sigma}_t^2$ is either periodical or converging to a constant C_1 . This represents the ‘‘best-case scenario’’ for an idealized model: regardless of how the original series fluctuates, it perfectly captures the true trend and noise distribution and faithfully propagates them to the next time step. In practical models, however, this property often leads to noise accumulation, which in turn distorts long-horizon forecasts.

C Baselines

In this section, we introduce a variety of representative baselines that span likelihood-based, perturbation-based, rank-based, and geometry-based detection strategies. These methods are carefully adapted to our time series scenario and we use consistent settings to ensure comparability, thereby providing a robust foundation for benchmarking.

C.1 DNA-GPT (WScore)

DNA-GPT WScore (Yang et al. 2024) measures the average similarity between the regenerated text and the original suffixes of the truncated input sequences. The approach is based on the hypothesis that, conditioned by a fixed prefix, the log-likelihood of the machine-generated remaining text substantially exceeds that of human-generated text. Operationally, DNA-GPT truncates each input sequence in a specified ratio, generates multiple continuations from the retained prefix, and evaluates the average difference in log-probability between the regenerated and original suffixes as the detection signal. In this study, we adopt the white-box version of DNA-GPT as a baseline since the black-box metric is inapplicable in the context of our problem.

We follow the original parameter configuration reported in (Yang et al. 2024). In particular, we set the truncation ratio (i.e., the proportion of regenerated tokens) to $\alpha = 0.5$, and the regeneration iterations to be 10.

C.2 DetectGPT

DetectGPT (Mitchell et al. 2023) builds on the hypothesis that LLM-generated text tends to lie in regions of negative curvature in the model’s log-probability landscape. As a result, such text is more sensitive to perturbations, exhibiting greater reductions in log-likelihood when rephrased or slightly modified, compared to human-written text. Building on this hypothesis, DetectGPT generates multiple semantically equivalent perturbations of the input sequence and compares the log-probability of the original sample with each perturbed sample. The perturbations are typically produced using pre-trained models such as T5, via operations like paraphrasing or word deletion that aim to preserve the input’s semantics. Note that the ‘‘black-box’’ version of DetectGPT assumes no access to the original generation model but still requires access to the logit distributions of a surrogate language model. In practice, this setup aligns with the zero-shot scenario considered in our experiments. Therefore, we treat it as a white-box method in this context.

In our adaptation of DetectGPT to time series data, perturbations are introduced by randomly selecting a subset of tokens and substitute them with alternatives from their local temporal neighborhood (within a window size of 2) to preserve semantics based on similarity. We set the perturbation ratio (i.e., the proportion of perturbed tokens) to $\beta = 0.3$ and generate 10 perturbations for each input sequence, consistent with the configuration used in the original work.

C.3 Fast-DetectGPT

Fast-DetectGPT (Bao et al. 2023) is a computationally efficient variant of DetectGPT that significantly reduces infer-

ence cost by computing log probabilities only for the perturbed tokens, rather than for the entire sequence. This selective computation strategy preserves and even improves detection performance while improving efficiency. In our experiment, we adopt the same parameter configuration as DetectGPT, with the perturbation ratio $\beta = 0.3$ and 10 perturbations generated for each input sequence.

C.4 DetectLLM

DetectLLM (Su et al. 2023) concentrates on the probability rank of tokens, and consists of two metrics, namely Log-Likelihood Log-Rank Ratio (LRR) and Normalized Perturbed log-Rank (NPR). LRR measures the average log probabilities of all tokens in the sample against the average log rank. NPR is based on the log rank difference between original and perturbed samples, where multiple semantically equivalent perturbations are generated, and the log rank differences between the original sequence and the perturbations are estimated.

In our adaptation of DetectLLM to time series data, perturbations are introduced in the same manner as DetectGPT for NPR method, and we follow the same parameter configuration as DetectGPT, with the perturbation ratio $\beta = 0.3$ and 10 perturbations generated for each input sequence.

C.5 Intrinsic Dimension

Intrinsic Dimension method (Tulchinskii et al. 2023) treats a sequence of tokens as a point cloud on a low-dimensional manifold in the embedding space and estimates its “persistent homology dimension” via topological data analysis (TDA). In particular, it measures the 0-dimensional persistence lifetimes by computing the total edge-length of the point cloud’s minimum spanning tree (MST).

Concretely, each token is mapped to a high-dimensional vector using a pre-trained Transformer encoder. In our adaptation of Intrinsic Dimension method to time series, we feed the entire prefix of a token into Chronos-T5 (large) and take its pooled embedding, since token semantics depend on the full context. We then apply the original parameter settings from (Tulchinskii et al. 2023):

- **Weight exponent** $\alpha = 1.0$: each MST edge length L contributes as $L^\alpha = L$.
- **Distance metric**: Euclidean distance in \mathbb{R}^n is used to build the MST.
- **Number of scales** $k = 8$: the range of sample sizes is partitioned into eight equally spaced values.
- **Subsampling per scale** $J = 7$: for each scale, seven random subsets are drawn and their MST lengths computed, with the median retained.
- **Repeat runs** $n = 3$: the slope is calculated three times to obtain the average slope and recover the intrinsic dimension.

C.6 FourierGPT

FourierGPT (Xu et al. 2024) generalizes from the uniform information density (UID) hypothesis from psycholinguistic, which posits that human language tends to distribute

information evenly across utterance. Unlike conventional white-box detectors that operate on raw token probabilities, FourierGPT analyze the spectrum of relative token likelihoods to better capture this linguistic property. This method posits that human-generated text exhibits lower low-frequency power in relative likelihood sequence than model-generated text. Leveraging this finding, both supervised and unsupervised classifiers are proposed for detection.

In our adaptation of FourierGPT to time series data, we perform the same normalization and frequency-domain decomposition to the likelihood sequence, and follow the unsupervised FourierGPT’s configuration to use the sum of the first ten low-frequency components’ magnitudes as the classifier.

C.7 Binocular

Binocular (Hans et al. 2024) proposes that the hidden context or prompt of text segments can introduce additional perplexity into the passage, thereby confusing the probability-based detectors and impairing their performance. To mitigate the contextual conditioning of text distributions, the Binocular method introduces an observer model. By measuring the cross-perplexity of texts under the probability distributions of both models, it reconstructs the text’s original perplexity independently of contextual bias.

In our adaptation of Binocular, we use Chronos-T5 (tiny) as the observer model and Chronos-T5 (large) as the performer model.

C.8 Traditional Metrics

Traditional metrics, including log-probability, rank and log rank (Gehrmann, Strobel, and Rush 2019; Jawahar, Abdul-Mageed, and Lakshmanan 2020; Solaiman et al. 2019), leverage the model’s logit distribution to quantify how likely each token is under the model.

D Supplementary Experiments and Results

D.1 Compute Resources and Hyperparameter Details

In this section we provide the computational environment and the selection of hyperparameters of the UCE method. All inference experiments were run on a single NVIDIA Tesla V100 GPU (approximately 3000 MiB of dedicated memory) with no additional training required.

Given a fixed time series length H , which typically takes the value of 64 in the main experiment, the value of the starting point t_1 is discussed in Section D.4, and typically $t_1 = 0.75 \cdot H$. We set $\Delta t = 1$, and therefore $N = H - t_1$. For $H = 64$, there is $N = 16$. When confining the neighborhood \mathcal{U} , we set the center of the neighborhood to be the mean value of the internal probability distribution $\mu = \sum_x x \cdot \hat{P}(x)$, and the radius of \mathcal{U} to be 50 under the size of the vocabulary to be $|\mathcal{V}| = 4096$. The selection of hyperparameters is highly flexible according to length H and vocabulary size $|\mathcal{V}|$.

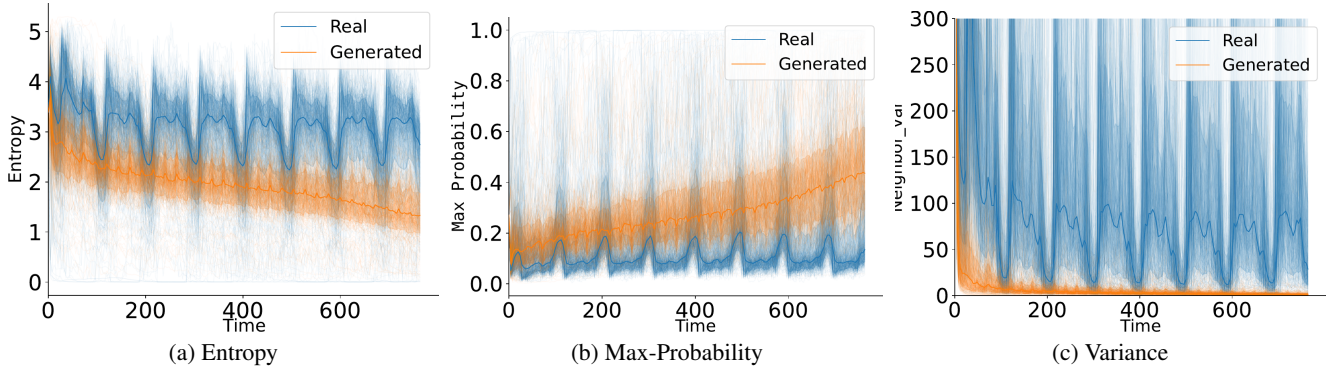


Figure 6: Uncertainty reduction for Timer-generated time series.

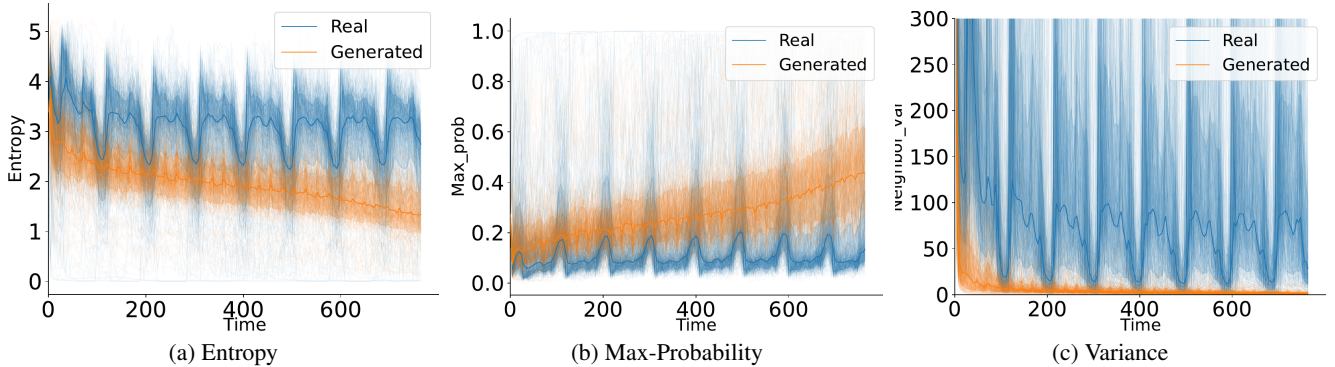


Figure 7: Uncertainty reduction for TimeMoE-generated time series.

D.2 Runtime Efficiency

We compare the runtime of different detection methods by measuring their average processing time per instance, as shown in Fig. 10. Among white-box methods, UCE achieves the second fastest runtime (0.47 s), significantly outperforming the baseline approaches such as DetectGPT (23.18 s), DetectLLM-NPR (22.93 s) and DNA-GPT (16.30 s). These methods require multiple resampling or perturbations, which introduce additional computation. Traditional statistical methods such as Log Likelihood (8.32 s), FourierGPT (8.35 s) and DetectLLM-LLR (8.32 s) that utilize Log Rank show moderate latency. These methods infer the logit distribution for every token for a single sequence, while Fast-DetectGPT (9.32 s) only infers the logit distribution over subsets of tokens across multiple perturbed sequences. Binocular requires simultaneous inference of the observer model and the performer model. With both models loaded in parallel (which is the optimal scenario), the runtime of this method (9.98 s) is determined by the slower of the two. Although both categories achieve substantial speedups, they lag behind UCE, which only computes a small portion (around 1/8) of token logits in a single sequence. Noting that the Intrinsic Dimension method requires a relatively small proportion of embeddings to estimate the persistent homology dimension, which leads to the fastest runtime (0.33 s). However, for stability in performance, multiple reruns are

often required (typically 3-10 times). This significantly increases the effective runtime to 1-3 seconds, reducing its nominal advantage. Therefore, even after adjusting for practical usage scenarios, UCE retains a clear advantage in both efficiency and real-world applicability.

D.3 Detection with Shorter Time Series Length

To test the robustness of UCE on relatively shorter input sequences, we conduct detection experiments on sequences with an average length of $H = 24$. According to the Contraction Hypothesis, shorter time series exhibit a smaller overall reduction in uncertainty, thereby degrading detection performance. This phenomenon aligns with previous findings in text generation detection that shorter texts are less discriminative.

As shown in Table 4, all methods experience a general drop in performance under this setting. Nevertheless, UCE maintains a consistent advantage in TPR for in-distribution datasets, while achieving comparable AUROC scores to the baselines. On zero-shot datasets, UCE sustains a slight but stable lead in both AUROC and TPR. These results demonstrate that UCE remains effective and relatively stable across varying sequence lengths, even under constrained temporal contexts.

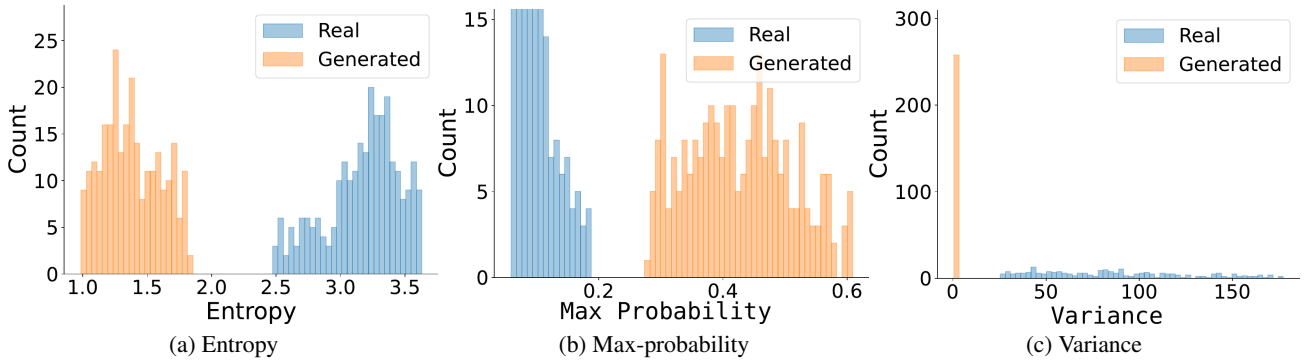


Figure 8: Uncertainty discrepancy for real (blue) and Timer-generated (orange) time series

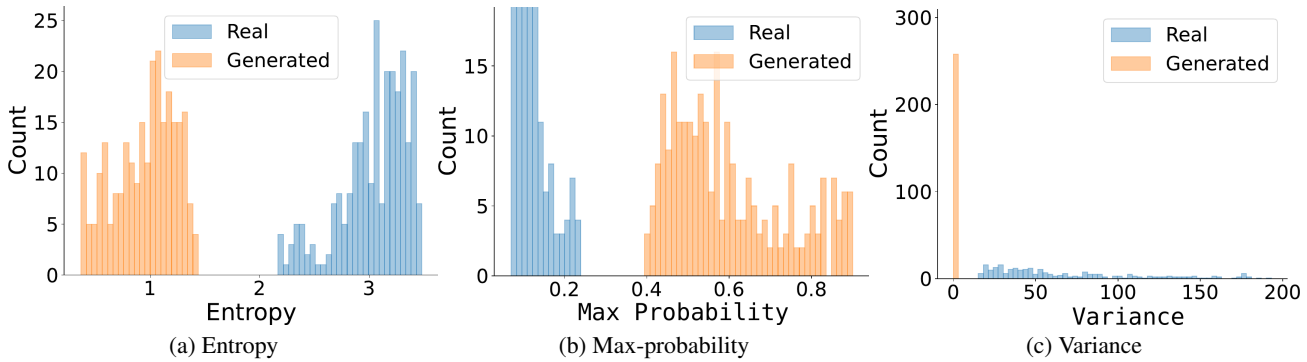


Figure 9: Uncertainty discrepancy for real (blue) and TimeMoE-generated (orange) time series.

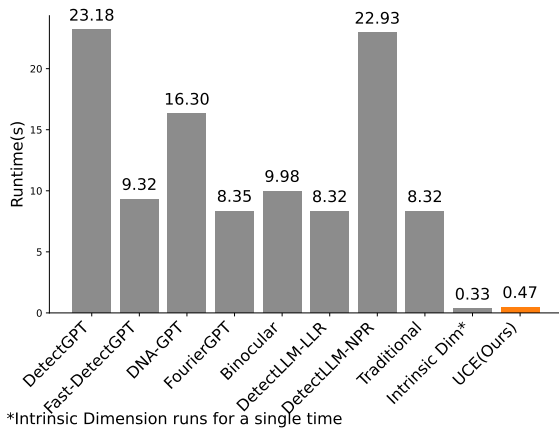


Figure 10: Runtime (in seconds) of different detection methods on a single input sequence. Although Intrinsic Dimension is shown with the shortest runtime, it typically requires multiple repeated runs to achieve stable results in practice. Overall, UCE is far more efficient, particularly when compared with white-box approaches.

D.4 Starting Point Analysis

The UCE methods evaluate the variation of uncertainty in time series with unknown history. This naturally give rise to

two important properties: (1) early prediction distributions tend to be unstable due to insufficient history; (2) the contraction of uncertainty is increasingly pronounced at later time points. Motivated by these observations, we adjust the evaluation window by excluding the initial prefix and delaying the starting point of prediction. Specifically, we set the forecasting start time to $t_0 = \alpha \cdot T$, and evaluate several values of $\alpha \in \{0, 0.25, 0.5, 0.75, 0.99\}$ to study its impact on detection performance. Note that setting $\alpha = 0.99$ corresponds to using only the final token to obtain the predictive distribution to calculate UCE metrics. The results, summarized in Fig. 11, show that as α increases, AUROC remains stable or improves slightly while TPR shows modest fluctuation.

Overall, detection performance is stable across a wide range of α values, suggesting that UCE is relatively robust to the choice of starting position. We therefore set $\alpha = 0.75$ in our main experiments to balance AUROC and TPR performance.

E Comparison between Textual and Temporal Data in Model Generation

Time Series Large Models share foundational similarities with LLMs as they both rely on Transformer based recursive prediction, yet their tokens differ fundamentally. Text tokens represent discrete semantic words or subwords whose mean-

Dataset	In-Domain Datasets Avg.		Zero-Shot Datasets Avg.	
	AUROC	TPR	AUROC	TPR
$\log p(x)$	0.730	0.101	0.640	0.171
Rank	0.734	0.115	0.615	0.147
LogRank	0.767	0.119	0.644	0.171
DetectGPT	0.620	0.032	0.631	0.105
Fast-DetectGPT	0.690	0.047	0.611	0.091
DetectLLM-LLR	<u>0.760</u>	0.213	0.645	0.159
DetectLLM-NPR	0.685	0.065	0.626	0.121
DNA-GPT	0.476	0.065	0.462	0.069
FourierGPT	0.528	0.030	0.505	0.013
Binocular	0.523	0.035	0.597	0.037
Intrinsic Dimension	0.600	0.105	0.536	0.041
SCS -Entropy	0.751	<u>0.264</u>	<u>0.692</u>	<u>0.199</u>
-Max Prob	0.749	0.277	0.703	0.211
-Variance	0.738	0.116	0.614	0.115

Table 4: AUROC and TPR (at 1% FPR) for detecting samples with shorter lengths. The **best** and **second-best** results are highlighted. There are declines in performance as the length decreases.

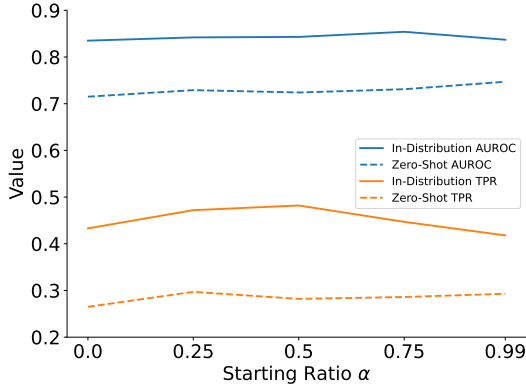


Figure 11: Effect of starting points $t_0 = \alpha \cdot T$ on AUROC and TPR in both dataset categories.

ings is derived through their semantic mapping to real-world entities or abstract concepts, and is reflected by the contextual relationships within texts. In contrast, continuous real-valued observations are discretized into a bounded ordered set, which preserves both the numerical ordering (e.g., token “1000” is 300 units greater than “700”) and metric similarity (e.g., token “490” is closer to “500” than “560”).

Time series tokens inherit the order and metric structure of real values, thereby carrying non-arithmetic semantic information. TSLMs implicitly learn these metric-based semantic relationships between tokens from the continuous nature of their training data, as high continuity of real-valued sequences preserves this underlying semantics, enabling the models to “internalize” and exploit this information in their forecasts. This means that each temporal token has many “semantic neighbors” with high metrical similarity to define a neighborhood. For instance, temperature 25.1°C, 25.2°C and 25.3°C all lie within a small numeric range. Their high similarity implies low information difference within this neighborhood. In other words, although a massive vocab-

ulary may span thousands of discrete values, only a small subset of these local neighborhoods defines clear semantic boundaries, which illustrates the sparse information density.

F Reevaluating Generation Detection for Time Series via Uncertainty

In this section, we reevaluate the baseline methods, which share two key traits with UCE: performance improves on longer series and on in distribution data. This suggests a lens of uncertainty from which to assess these baselines.

Point-wise probabilities fail to capture overall uncertainty in time series forecasts, and relevant methods (e.g. $\log p$ and DNA-GPT) tend to underperform. The probability of individual output token is less effective in reflecting the model’s entire internal probability distribution. The arbitrary nature of time series values causes a smoothed internal probability distribution at each time point, and the token-wise probability differences are low. In terms of uncertainty, a low $p(x_t)$ may reside in the tail of a peaked distribution or the body of a flat one, offering minimal discriminative power. However, a higher probability is more informative by approximating the maximum probability.

Perturbation-based methods (DetectGPT, Fast DetectGPT, NPR) detect generation by measuring how output scores change when a few tokens are swapped with semantic neighbors. In time series, replacing a small fraction of values adds noise of variance σ_N^2 on top of the inherent series variance σ_I^2 . The resulting score change—whether a likelihood ratio or a log rank difference—depends critically on σ_N^2 against σ_I^2 . If $\sigma_N^2 \ll \sigma_I^2$, the perturbation is too weak to detect; if $\sigma_N^2 \gg \sigma_I^2$, the noise overwhelms the original pattern. Moreover, varying σ_I^2 across datasets makes it difficult to choose a single perturbation strength that works universally.

Rank-based metrics invert token probability: a lower numeric rank indicates lower uncertainty. In principle, rank captures how concentrated the predictive distribution is around its top candidates. However, in time series forecasting most token probabilities are uniformly low, so ranks cluster at high values with little variation, making rank alone a weak signal for distinguishing generated from real data.

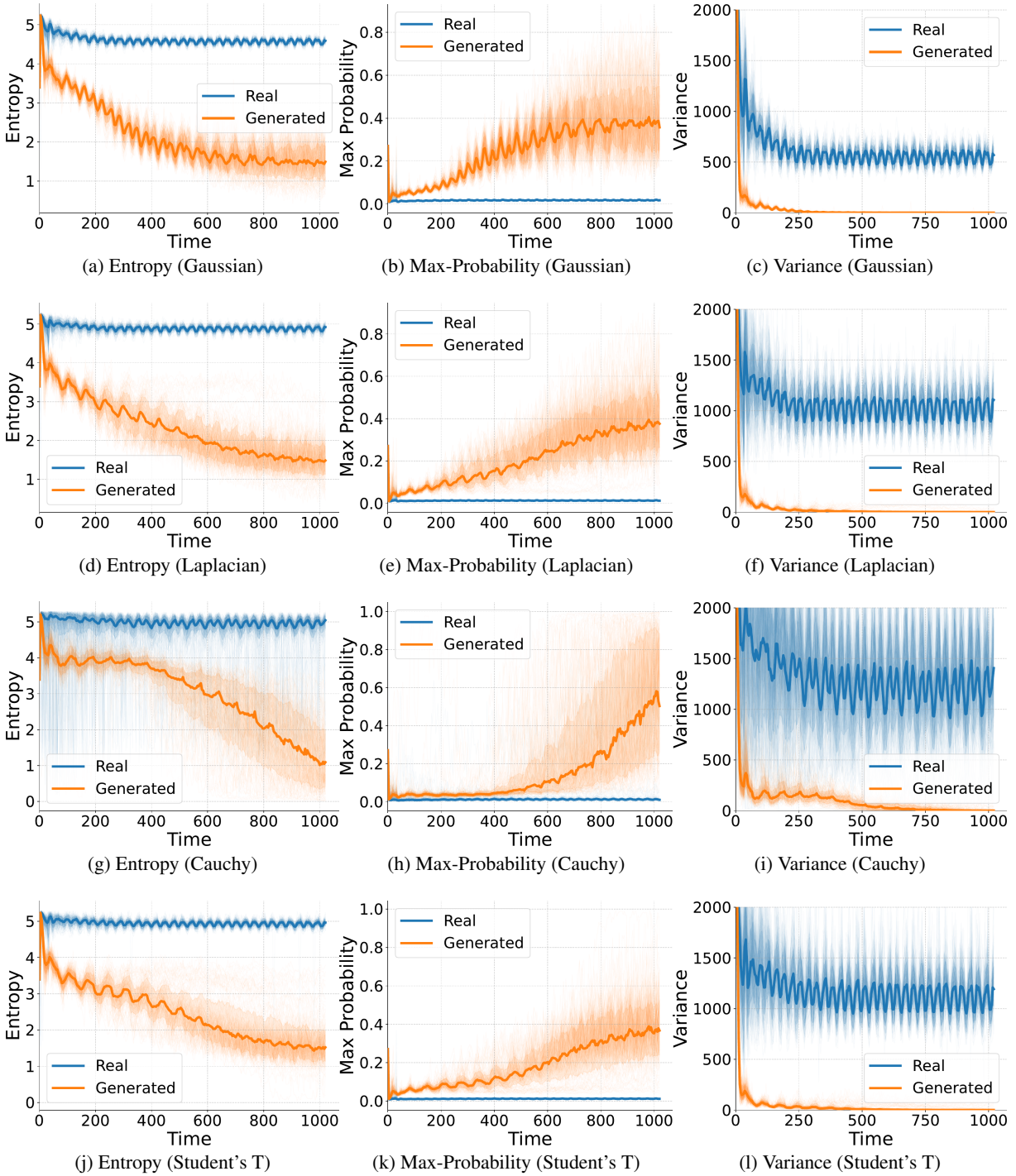


Figure 12: Difference of entropy between real and model-generated data for various types of noise distributions on sine waves.

Dataset	Electricity (15M)		Electricity (H)		Electricity (W)		KDD Cup		LDN SmtMeter		M4 (H)	
	AUROC	TPR	AUROC	TPR	AUROC	TPR	AUROC	TPR	AUROC	TPR	AUROC	TPR
$\log p(x)$	0.449	0.014	0.819	0.140	0.667	0.125	0.472	0.000	0.822	0.017	0.730	0.614
Rank	0.473	0.035	0.663	0.081	0.727	0.137	0.583	0.000	0.863	0.029	0.800	0.597
LogRank	0.529	0.019	0.800	0.115	0.691	0.156	0.639	0.167	0.869	0.046	0.773	0.614
DetectGPT	0.404	0.016	0.453	0.025	0.760	0.072	0.444	0.000	0.676	0.013	0.507	0.027
Fast-DetectGPT	0.463	0.014	0.733	0.087	0.691	0.165	0.417	0.000	0.796	0.017	0.515	0.220
DetectLLM-LLR	0.727	0.141	0.856	0.093	0.637	0.087	0.667	0.167	0.863	0.209	0.798	0.594
DetectLLM-NPR	0.515	0.024	0.844	0.072	0.676	0.047	0.417	0.000	0.748	0.039	0.744	0.548
DNA-GPT	0.599	0.038	0.808	0.162	0.772	0.022	0.500	0.500	0.807	0.029	0.595	0.107
Intrinsic Dimension	0.545	0.068	0.867	0.018	0.733	0.006	0.800	0.200	0.603	0.018	0.461	0.415
FourierGPT	0.485	0.019	0.360	0.000	0.246	0.006	0.778	0.667	0.534	0.014	0.623	0.094
Binocular	0.278	0.005	0.284	0.000	0.708	0.009	0.389	0.000	0.762	0.022	0.491	0.002
UCE-Entropy	0.766	0.070	0.797	0.037	0.803	0.349	0.972	0.833	0.924	0.467	0.686	0.384
-Max Prob	0.728	0.084	0.756	0.019	0.818	0.343	0.972	0.833	0.879	0.341	0.682	0.382
-Variance	0.826	0.154	0.883	0.118	0.836	0.352	0.806	0.500	0.935	0.351	0.661	0.616

Dataset	Pedestrian		Rideshare		Taxi		Temperature		Uber TLC (D)		Uber TLC (H)		Top-2 Count	
	AUROC	TPR	AUROC	TPR										
$\log p(x)$	0.985	0.848	0.648	0.000	0.854	0.039	0.864	0.001	0.872	0.000	0.778	0.031	0	2
Rank	0.896	0.561	0.636	0.000	0.897	0.147	0.868	0.002	0.851	0.000	0.821	0.015	1	0
LogRank	0.981	0.894	0.652	0.000	0.921	0.186	0.877	0.011	0.879	0.000	0.871	0.034	1	0
DetectGPT	0.174	0.015	0.617	0.000	0.653	0.008	0.858	0.000	0.311	0.000	0.666	0.057	0	0
Fast-DetectGPT	0.954	0.591	0.636	0.000	0.812	0.010	0.879	0.000	0.877	0.000	0.774	0.050	0	0
DetectLLM-LLR	0.992	0.970	0.659	0.090	0.944	0.425	0.867	0.405	0.892	0.271	0.883	0.431	4	3
DetectLLM-NPR	0.984	0.788	0.619	0.007	0.722	0.003	0.836	0.003	0.846	0.000	0.772	0.019	0	0
DNA-GPT	0.747	0.091	0.417	0.000	0.444	0.000	0.528	0.000	0.592	0.000	0.460	0.027	0	1
Intrinsic Dimension	0.932	0.343	0.521	0.015	0.683	0.013	0.572	0.005	0.724	0.252	0.561	0.074	0	0
FourierGPT	0.366	0.000	0.590	0.012	0.434	0.006	0.626	0.011	0.637	0.008	0.667	0.038	0	1
Binocular	0.439	0.000	0.569	0.004	0.446	0.002	0.842	0.144	0.662	0.004	0.626	0.015	0	0
UCE-Entropy	0.986	0.909	0.700	0.039	0.963	0.470	0.960	0.817	0.926	0.500	0.773	0.489	8	6
-Max Prob	0.985	0.909	0.649	0.088	0.960	0.483	0.935	0.711	0.930	0.576	0.790	0.519	5	6
-Variance	0.980	0.924	0.733	0.026	0.936	0.377	0.924	0.418	0.898	0.015	0.770	0.046	6	5

Table 5: Full result of AUROC and TPR (at 1% FPR) for detecting samples on In-Distribution Datasets. The **best** and **second-best** results are highlighted.

Dataset	Aus EI Demand		CIF 2016		Covid Death		ERCOT		ETTh		ETTm		Exchange Rate	
	AUROC	TPR	AUROC	TPR	AUROC	TPR	AUROC	TPR	AUROC	TPR	AUROC	TPR	AUROC	TPR
$\log p(x)$	0.480	0.400	0.872	0.361	0.576	0.098	0.734	0.375	0.653	0.286	0.209	0.071	0.859	0.000
Rank	0.880	0.400	0.861	0.569	0.576	0.026	0.742	0.375	0.497	0.214	0.273	0.071	0.883	0.250
LogRank	0.600	0.200	0.889	0.639	0.574	0.030	0.805	0.625	0.658	0.286	0.260	0.143	0.875	0.250
DetectGPT	0.560	0.400	0.697	0.017	0.573	0.045	0.672	0.250	0.505	0.000	0.230	0.000	0.859	0.000
Fast-DetectGPT	0.520	0.400	0.908	0.700	0.561	0.026	0.641	0.250	0.684	0.357	0.209	0.000	0.828	0.000
DetectLLM-LLR	0.680	0.400	0.905	0.600	0.539	0.015	0.828	0.375	0.923	0.357	0.413	0.143	0.859	0.750
DetectLLM-NPR	0.520	0.400	0.915	0.500	0.586	0.004	0.781	0.500	0.934	0.571	0.173	0.000	0.844	0.125
DNA-GPT	0.280	0.000	0.481	0.032	0.374	0.004	0.516	0.250	0.811	0.643	0.684	0.358	0.250	0.000
Intrinsic Dimension	0.600	0.400	0.744	0.250	0.474	0.022	0.440	0.000	0.630	0.300	0.540	0.100	0.400	0.000
FourierGPT	0.720	0.400	0.644	0.014	0.653	0.004	0.719	0.125	0.414	0.000	0.541	0.071	0.797	0.250
Binocular	0.200	0.000	0.641	0.028	0.618	0.139	0.781	0.625	0.480	0.214	0.541	0.071	0.266	0.125
UCE-Entropy	0.680	0.400	0.915	0.625	0.540	0.023	0.586	0.125	0.770	0.571	0.561	0.214	0.891	0.375
-Max Prob	0.760	0.600	0.876	0.611	0.543	0.023	0.555	0.125	0.694	0.500	0.546	0.214	0.859	0.375
-Variance	0.640	0.400	0.902	0.431	0.451	0.038	0.555	0.125	0.760	0.643	0.536	0.214	0.016	0.000

Dataset	Fred MD		Hospital		M1 (M)		M1(Q)		M3 (M)		M3 (Q)		M4(Q)	
	AUROC	TPR												
$\log p(x)$	0.709	0.075	0.915	0.527	0.783	0.000	0.372	0.000	0.758	0.118	0.278	0.000	0.235	0.000
Rank	0.706	0.121	0.882	0.437	0.735	0.000	0.301	0.000	0.665	0.054	0.230	0.000	0.993	0.790
LogRank	0.697	0.121	0.917	0.562	0.788	0.000	0.317	0.000	0.717	0.148	0.242	0.000	0.238	0.000
DetectGPT	0.687	0.028	0.872	0.029	0.726	0.006	0.645	0.000	0.736	0.092	0.398	0.000	0.000	0.000
Fast-DetectGPT	0.709	0.084	0.909	0.544	0.829	0.008	0.610	0.000	0.720	0.197	0.329	0.000	0.000	0.000
DetectLLM-LLR	0.682	0.252	0.906	0.437	0.779	0.029	0.399	0.000	0.624	0.160	0.298	0.000	0.421	0.000
DetectLLM-NPR	0.694	0.075	0.888	0.182	0.806	0.000	0.558	0.000	0.707	0.117	0.307	0.000	0.230	0.000
DNA-GPT	0.309	0.009	0.265	0.000	0.557	0.000	0.398	0.000	0.469	0.009	0.408	0.000	0.446	0.000
Intrinsic Dimension	0.607	0.127	0.436	0.026	0.807	0.071	0.898	0.248	0.729	0.105	0.941	0.453	0.670	0.227
FourierGPT	0.520	0.000	0.584	0.017	0.535	0.006	0.358	0.005	0.600	0.071	0.323	0.000	0.981	0.623
Binocular	0.443	0.028	0.386	0.004	0.594	0.044	0.728	0.005	0.593	0.130	0.747	0.012	0.877	0.000
UCE-Entropy	0.582	0.234	0.903	0.660	0.785	0.008	0.585	0.005	0.616	0.233	0.449	0.000	0.345	0.000
-Max Prob	0.567	0.215	0.898	0.681	0.768	0.032	0.624	0.025	0.595	0.256	0.491	0.001	0.356	0.000
-Variance	0.449	0.121	0.894	0.627	0.744	0.000	0.325	0.000	0.614	0.124	0.167	0.000	0.382	0.000

Dataset	M5		NN5 (W)		Tourism (M)		Tourism (Q)		Traffic		Weather		Top-2 Count	
	AUROC	TPR	AUROC	TPR										
$\log p(x)$	0.695	0.009	1.000	1.000	0.902	0.005	0.875	0.002	0.567	0.074	0.641	0.002	4	3
Rank	0.748	0.005	0.901	0.622	0.856	0.161	0.854	0.000	0.624	0.079	0.651	0.001	4	2
LogRank	0.758	0.006	1.000	1.000	0.909	0.232	0.888	0.000	0.592	0.082	0.661	0.001	3	2
DetectGPT	0.649	0.004	1.000	0.991	0.912	0.003	0.895	0.007	0.636	0.048	0.646	0.003	2	2
Fast-DetectGPT	0.659	0.005	0.999	0.991	0.913	0.011	0.903	0.012	0.629	0.013	0.647	0.005	4	3
DetectLLM-LLR	0.816	0.145	0.979	0.730	0.909	0.123	0.807	0.027	0.526	0.052	0.811	0.066	2	4
DetectLLM-NPR	0.654	0.005	0.998	0.946	0.880	0.005	0.821	0.000	0.496	0.049	0.644	0.006	2	2
DNA-GPT	0.510	0.003	0.694	0.081	0.725	0.000	0.657	0.000	0.818	0.065	0.217	0.002	1	2
Intrinsic Dimension	0.572	0.001	0.662	0.050	0.635	0.070	0.643	0.028	0.695	0.014	0.940	0.595	4	4
FourierGPT	0.621	0.015	0.452	0.000	0.583	0.008	0.525	0.005	0.409	0.001	0.836	0.025	2	2
Binocular	0.682	0.009	0.717	0.063	0.614	0.003	0.790	0.084	0.670	0.082	0.874	0.004	3	5
UCE-Entropy	0.726	0.119	1.000	1.000	0.973	0.620	0.921	0.033	0.895	0.375	0.899	0.108	8	12
-Max Prob	0.740	0.118	1.000	1.000	0.970	0.604	0.936	0.199	0.895	0.421	0.899	0.119	6	11
-Variance	0.807	0.018	1.000	1.000	0.973	0.658	0.882	0.000	0.859	0.147	0.721	0.001	4	5

Table 6: Full result of AUROC and TPR (at 1% FPR) for detecting samples on Zero-Shot Datasets. The **best** and second-best results are highlighted.